Development of a Defect-controlled Rapid 3D Printing System for Flexible Plastic Materials

by

Wonchul Lee

B.A.Sc., Simon Fraser University, 2020

Thesis Submitted in Partial Fulfillment of the
Requirements for the Degree of
Master of Applied Science

in the
School of Mechatronic Systems Engineering
Faculty of Applied Sciences

SIMON FRASER UNIVERSITY
Spring 2023

Declaration of Committee

Name:	**Wonchul Lee**
Degree:	**Master of Applied Science**
Title:	**Development of a Defect-controlled Rapid 3D Printing System for Flexible Plastic Materials**
Committee:	**Chair:** **Helen Bailey** Lecturer, Mechatronic Systems Engineering
	Woo Soo Kim Supervisor Professor, Mechatronic Systems Engineering
	Gary Wang Committee Member Professor, Mechatronic Systems Engineering
	Lawrence Kim Examiner Assistant Professor, Computing Science

Abstract

Material extrusion or fused deposition modeling is a popular 3D printing process that currently faces challenges in processing flexible materials such as thermoplastic polyurethane regarding printability and fabrication performance. It has been observed that naturally occurring printing defects, such as stringing and blobs, have a significant impact on the mechanical properties of the prints. To address these challenges, this study presents a system that utilizes a convolutional neural network to control defects in real-time, while simultaneously ensuring the printability of flexible materials through precise parameter control. The proposed system autonomously controls printing parameters such as flow rate and nozzle temperature. Results show that the system can correct stringing and blobs defects within 25 printing layers and reduce printing time by up to 30% while keeping the mechanical strength within an error range of 3.18%. This system has the potential to improve efficiency and reduce waste in advanced 3D printing technologies.

Keywords: 3D printing; Material extrusion; Finite deposition modeling; Convolutional neural networks; Machine learning; Computer vision

I would like to dedicate this thesis to my loving family

Acknowledgements

First and foremost, I would like to show my sincere gratitude to my senior supervisor Dr. Woo Soo Kim. Without him, none of this would have been possible. His academic guidance and comments have been really valuable to me. I am truly grateful for the opportunity to learn and proceed with my graduate studies under his supervision. Throughout the long journey of two years, his words strongly encouraged and inspired me with research studies.

I would also like to further appreciate my supervisory committee, Dr. Gary Wang for his valuable feedback and suggestions that contributed heavily towards the development and improvement of my research project. Moreover, I would like to thank Dr. Lawrence Kim and Dr. Helen Bailey for their time and consideration of my research study.

My family has always been the strongest support in my life. I am always grateful for the love I received from you all. You encouraged me to continue my study, find passion and prayed for my well-being. Thank you for trusting me and being on my side throughout this journey and my life.

To my brothers and friends from my life and Additive Manufacturing Lab, Antsun, Minku, Ho-Young, Amir, Chao, Hadi, Haotian, and Tae-Ho. Everyone has supported me in this journey, and I am truly fortunate to have met you all in my life.

Table of Contents

List of Tables

List of Figures

List of Acronyms

ABS	Acrylonitrile Butadiene Styrene
AI	Artificial Intelligence
AM	Additive Manufacturing
ANN	Artificial Neural Network
BA	Bootstrapped Aggregation
BN	Bayesian Networks
BRNN	Bidirectional Recurrent Neural Networks
CAN	Conditional Adversarial Network
CBAM	Composite Based Additive Manufacturing
CNN	Convolutional Neural Networks
DED	Directed Energy Deposition
DLP	Digital Light Processing
DLP	Directional Light Processing
DMD	Direct Metal Deposition
DOD	Drop-On Demand
EBM	Electron-Beam Melting
FDM	Fused Deposition Modelling
FFF	Fused Filament Fabrication
J48	J48 Decision Trees
LOM	Laminated Object Manufacturing
LPBF	Laser Powder Bed Fusion
LSTM	Long Short-Term Memory
NBC	Naïve Bayes Classifier
NN	Neural Networks
NPJ	Nanoparticle Jetting
PEEK	Polyetheretherkeytone
PEI	Polyetherimide
PLA	Polylactic Acid
PSL	Plastic Sheet Lamination

RBM	Restricted Boltzmann Machine
RNN	Recurrent Neural Networks
SLA	Stereolithography
SLM	Selective Laser Melting
SVM	Support Vector Machines
TCA	Transfer Component Analysis
TPU	Thermoplastic Polyurethane
TSVM	Transfer Support Vector Machine

Chapter 1. Introduction

1.1. Background

Additive Manufacturing (AM), so called 3D printing, is a process which enables the creation of complex, three-dimensional objects through the building layers of materials, such as plastic or metal, in a precise and controlled manner [1]. The process had experienced a remarkable expansion with first commercialization in year 1980 by Charles Hull [2]. In recent years, there has been a substantial growth in the development of 3D printing technologies. The advancements in 3D printing technology have led to its integration into a variety of industries including healthcare [3], aerospace [4], automotive [5], etc. The adoption of 3D printing technology in industrial manufacturing has brought several advantages over traditional manufacturing methods.

Artificial Intelligence (AI) is defined to be imitation of intelligent behaviour using computing devices which can be divided into two categories: systems that think and act like human and systems that think and act rationally [6]. Today, AI is one of the core drivers of the industrial processes and a critical factor in emerging technologies in the new innovations of data analysis. Over the period of 1961–2018, the AI has shown the broad capability of its applications from oil consumption forecast [7], weather forecast [8], medical educations [9, 10], etc. [11]. Despite the considerable number of issues with the implementation of artificial intelligence, it has emerged as a disruptive and transformative technology, providing support in various domains and industries.

1.1.1 Additive Manufacturing

One of the key advantages of AM process is the ability to produce customized, complex parts and products in a timely and efficient manner. Traditional manufacturing methods, such as injection molding or CNC machining, often encounter limitations in their ability to produce unique or intricate designs due to feasibility concerns. With 3D printing, however, designs can easily be modified and optimized to meet the specific needs of a given application, making it particularly useful for small-batch production and prototyping [12]. Other terms are used as synonyms for AM including desktop manufacturing, rapid manufacturing, and agile tooling on-demand manufacturing [13]. The process of AM is generally divided into three steps, modelling, printing, and finishing [14].

Prior to the AM process, the creation of 3D structure or the geometrical data of the desired object is required. This is typically done through computer-aided design (CAD) modeling processes [15, 16, 17]. The detailed and accurate representation of the desired objects including all specifications and dimensions required for printing can be created with it. Alternatively, 3D scanning technology can be used to import existing physical objects into the digital realm allowing them to be used as the basis of the 3D designs [18, 19]. Then, the created designs are used as the blueprint for the rapid prototyping processes. Overall, the 3D modelling process is critical for the successful additive manufacturing process as it lays the foundation for the accuracy and precision of the final product.

The printing process is the main process of the AM. After the creation of 3D model of the desired objects, the model needs to be converted into the data including geometrical information known as G-code. For this process, the 3D model needs to be converted using software known as “slicers” where it converts 3D models into a series of thin layers to create path for the motion of printer nozzle [20, 21]. The 3D printer then follows the G-code instructions to extrude layers of liquid or powder to build layers of cross-sections of the model. Then, each layer are joined or fused to create the final 3D model with its advantage of ability to create any complex 3D structures.

Although the resolution of printed models is sufficient for many applications based on its initial setting, printing process slightly changes the size due to its accuracy and precision error from the printer. Then, the post-processing such as surface treatment or removing support structures can be applied onto the printed model to increase the quality of the model.

1.1.2. Artificial Intelligence

The field of AI can be broadly categorized into two distinct approaches based on their philosophical underpinnings: strong and weak AI [22]. The strong AI refers to the idea that the machines can be designed to mimic human-like cognitive abilities and perform tasks that were once considered to be exclusive domains of humankind. The goal of the strong AI is to create systems that can perform intelligent tasks in a manner that is indistinguishable from human-like reasoning. To test the performance of the developed AI, the test known as Turning Test can be conducted where it is not operational definitions

based rather is inductive to show its good inductive grounds for thinking process [23]. Furthermore, it is stated that even if the strong AIs pass the Turning Test, it may be far from exhibiting a human-like mindsets and behaviours [24].

Weak AI on the other hand, is focused on the development of systems that can perform specific intelligent tasks through the learning process. The primary aim is to design machines that can perform these tasks efficiently and effectively. The weak AI emphasizes the use of machine learning algorithms and statistical models to enable systems to minimize human effort. One key benefit is that it is more practical and achievable in the shorter term, and it can have a significant impact on various industries or field of studies. For example, weak AI shows wide range of applications such as image and speech recognition [25, 26], customer service chatbots [27], witness expert system [28], smart driving system [29], etc. [30]. By automating the time-consuming tasks, weak AI is widely used to improve efficiency and productivity while freeing up human resources to focus on more complex and value adding tasks.

1.2. Motivation

The market size of 3D printing technology has been rapidly expanding, making it more accessible to both industries and end-users. Despite its widespread adoption, there are three major challenges faced by the technology: the quality and speed of printing complex models, and the printability of flexible materials such as Thermoplastic Polyurethane (TPU) or nylon. Currently, most 3D printing models are fabricated using rigid materials such as Polylactic Acid (PLA) and Acrylonitrile Butadiene Styrene (ABS) due to their processing simplicity.

One potential solution to the issue of flexible material printing is the integration of a machine vision system on the commercial 3D printers, with support from AI systems. This approach would enable the detection and correction of defects during the printing process. Currently, there are limited solutions to address this problem.

This research aims to develop a solution that can ensure printability while maximizing the printing speed and simultaneously detecting and correcting defects in the flexible material printing process. Ultimately, this work would contribute to the advancement of 3D printing technology in industries that require high-quality output, such

as aerospace and healthcare, by enabling the printing of complex structures with flexible materials.

1.3. Objectives and Scope

This research project aims towards developing the intelligent 3D printing system by utilizing computer vision and artificial intelligence specifically for the flexible material. The system aims to adjust printing parameters in real-time to correct detected defects while ensuring the printability of the flexible materials. The printing speed will be controlled based on the batch-printing-process where the printing speed is increased each batch of print and the correction data from previous batch will be applied to the new batch. The objectives of this research project are as follows:

1. Selecting suitable 3D structures for compression testing that clearly present variations in response to changes in printing parameters.
2. Identifying primary and secondary printing parameters to be controlled in real-time to ensure print quality and printability.
3. Setting up a computer vision system with strategically placed image sensor.
4. Designing the Convolutional Neural Networks (CNN) model for defect classification based on image data collected during printing.
5. Creating a parameter control system that responds to real-time image data classification results.
6. Developing a G-code update algorithm that increases printing speed while applying real-time correction data from previous print batches.

1.4. Contributions

For this research, Additive Manufacturing Laboratory (AML) at Simon Fraser University has extended the studies in 3D printing system and its applications. This research creates the foundation for the smart 3D printing system in the laboratory. In this research, the developed system demonstrated increasing the quality and time-efficiency of the commercial 3D printing system with flexible materials, TPU. This research has also been supported by the following publications:

- **W. Lee**, W. S. Kim "Self-controlled Yet Fast 3D Printing with Flexible Thermoplastic Polyurethane Materials" *Submitted*, 2023
- C. Bao, H. Moeinnia, T. H. Kim, **W. Lee** and W. S. Kim "3D Structural Electronics via Multi-directional Robot 3D Printing" *Advanced Materials Technologies* 2201349, 2022.
- **W. Lee**, J. Fritsch, A. Maqsood, S. Liu, T. Bourassa, R. Calara and W. S. Kim, "Adaptive 3D Printing for In Situ Adjustment of Mechanical Properties", *Advanced Intelligent Systems*, 2200229, 2022.
- T. H. Kim, X. Min, D. Baker, **W. Lee** and W. S. Kim, "3D architectured air sensing tubes for a portable mechanical ventilator", *Flexible and Printed Electronics*, vol. 6, no. 3, p. 035010, 2021

1.5. Thesis Overview

This thesis investigates the development of an intelligent 3D printing system for flexible materials, including computer vision, neural network design, and control systems. Chapter 2 provides background information on the current state of additive manufacturing processes with artificial intelligence systems, along with specific applications. Chapter 3 describes the development of the intelligent 3D printing system, including both hardware and software setup. Chapter 4 presents testing results for the developed neural network design, defect control capability, and printing speed optimization system. Chapter 5 provides a summary of the research project and outlines potential future applications and improvements for the developed system.

Chapter 2. Literature Review

2.1. Additive Manufacturing Processes

In the consideration of commercially available AM fabricators or devices, AM technologies are generally categorized into seven groups: VAT photopolymerization, Material jetting, Binder jetting, Powder Bed Fusion, Sheet lamination, Directed Energy Deposition (DED), and Material extrusion [31]. Each technology differs from another in the manner of the application process, material curing principle, and the initial state of the material.

The VAT photopolymerization process utilizes the ultraviolet (UV) light and photopolymers, which is light-curable resin to create desired 3D structures. Three key elements of the photopolymer mixture are monomers, oligomers, and photoinitiators where the photoinitiators release catalysts for the chain formation process between monomers and oligomers when exposed to the curing light [32, 33]. Some of the well-known printing processes are Stereolithography (SLA) and Digital Light Processing (DLP). The Material jetting process creates parts by depositing droplets of liquid photopolymers using piezo printing heads. It is prominent AM method in the polymer printing due to its advantages with high-precision printing for the thin layer thickness features with the thickness can be as low as 16 μm [34, 35, 36]. Some of the well-known printing processes are PolyJet, Nanoparticle Jetting (NPJ), and Drop-On Demand (DOD). Binder jetting dispenses liquid binding agents on powder to form a two-dimensional pattern on a layer. A wide variety of materials such as polymers, ceramics, and metals have been processed successfully with it [37, 38]. Similarly, the 3D structures are created through bonding the successive layers of material through the heat input in the powder bed fusion process. The printing type Selective Laser Sintering (SLS) shares similar printing process where SLS uses laser to bond powders and Binder jetting uses an industrial printhead that selectively deposits a liquid binding agent onto the powder bed [39, 40]. The sheet lamination process is developed with the basis of one of the first commercialized AM techniques, Laminated Object Manufacturing (LOM) in 1991. The process develops 3D structures using sheet layers with inclusion of prefabricated components between layers for deposition process [41, 42]. Other than LOM, few well-known sheet lamination technique-based printing processes are Plastic Sheet Lamination (PSL) and Composite

Based Additive Manufacturing (CBAM). DED is one of the promising flexible manufacturing technologies due to direct fabrication characteristics of complex structures. It can print layers on even and uneven substrates through its line-by-line deposition process [43, 44]. Some of the well-known DED technique-based 3D printing processes are Directional Light Processing (DLP) and Direct Metal Deposition (DMD).

2.1.1. Material Extrusion

The material extrusion is one of the most widely used 3D printing processes which involves the material from a spool of filaments that is loaded into the printer. The filaments then are melted to form a semi crystalline polymer above the glass transition temperature (T_g) and its melting temperature (T_M) [45]. The well-known material extrusion-based printing techniques are Fused Filament Fabrication (FFF) or Fused Deposition Modelling (FDM) [46]. Both systems create 3D structures by deposition of thin layers with filaments through the heated nozzle on the building plate. The nozzle extracts a thin layer of molten filaments onto the plate and stack the printed layers [47]. The system is broadly used in multiple disciplines due to its simplicity of usage and wide range of compatible materials such as soft to rigid plastics or polymers, ceramics, and metals [48].

There are two types of designs of the tool head: Direct Drive and Bowden [49, 50]. The main difference between the two tool heads is the location of the driving motor that pushes filament through the system. The direct drive design has motor mounted on the tool head gaining stronger extrusion force at a cost of nozzle stability due to inertia. The Bowden, however, has motor mounted on the printer chassis gaining the nozzle stability at the cost of losing extrusion force.

The direct drive is the most popular tool head design that is used in the market. As shown in the Figure 2.1, the direct drive extruder head consist of three core components: driving gear, guide roller, and hot end (heater). The printing process begins with the gripping of solid filament in between the gear and idle roller. The gear provides adequate force to push the filament in the hot end for the melting to extrusion process. The hot end consists of cylindrical ceramic cartridge heater that heats the aluminum heating box with thermistor for temperature sensing.

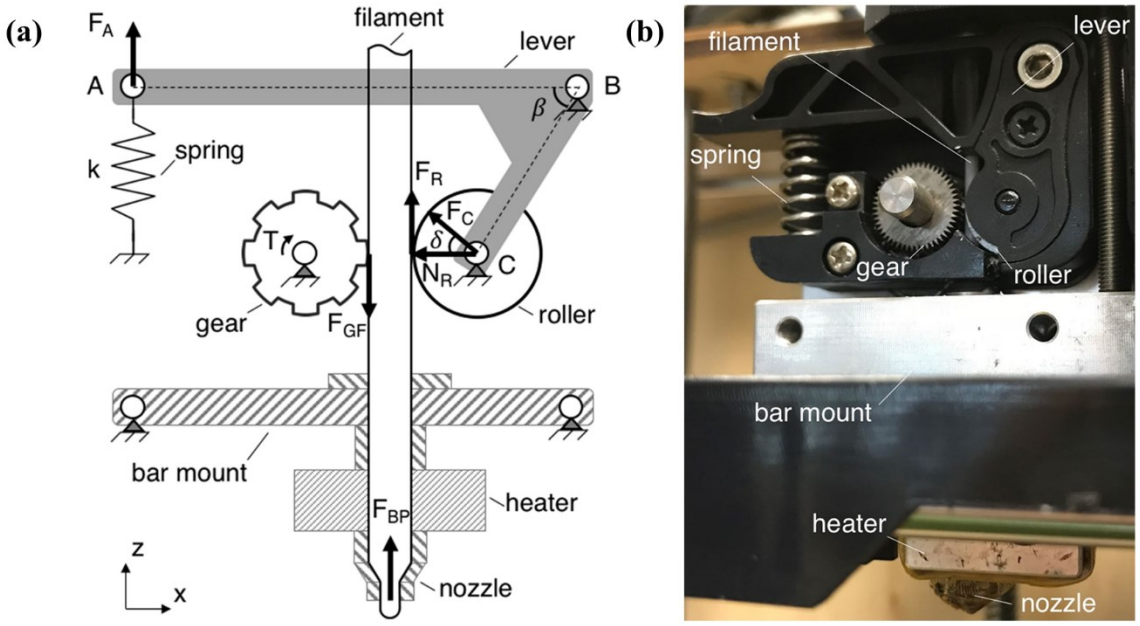

Figure 2.1. (a) The detailed schematic of the direct drive FDM extruder head. (b) The photo view of the common direct drive FDM extruder head. Reproduced with permission [51].

Within FDM, there are different types of printer designs such that the fabrication process dimension is not limited to 3-axis rather extends towards 6-axis. Few of new methods were investigated to overcome the disadvantages of the commercial 3-axis based 3D printers. 5-axis support-free 3D printing technologies were presented as shown in the Figure 2.2a,b. Mainly, two different approaches were found for 5-axis 3D printing technique: adding the stationary print plate [52, 53] or adding increased degree-of-freedom to the motion of the nozzle [54, 55]. Even if the 5-axis 3D printing techniques allow minimizing the support printed for the complex or curve-based structures, there is still limitation of the print size. Generally, with 3-axis or 5-axis 3D printers, the size of the printable structures are limited to chassis size of the printer. To further overcome the disadvantage, the 3D printing system utilizing the robotic arms were studied as shown in Figure 2.2c [56, 57, 58, 59].

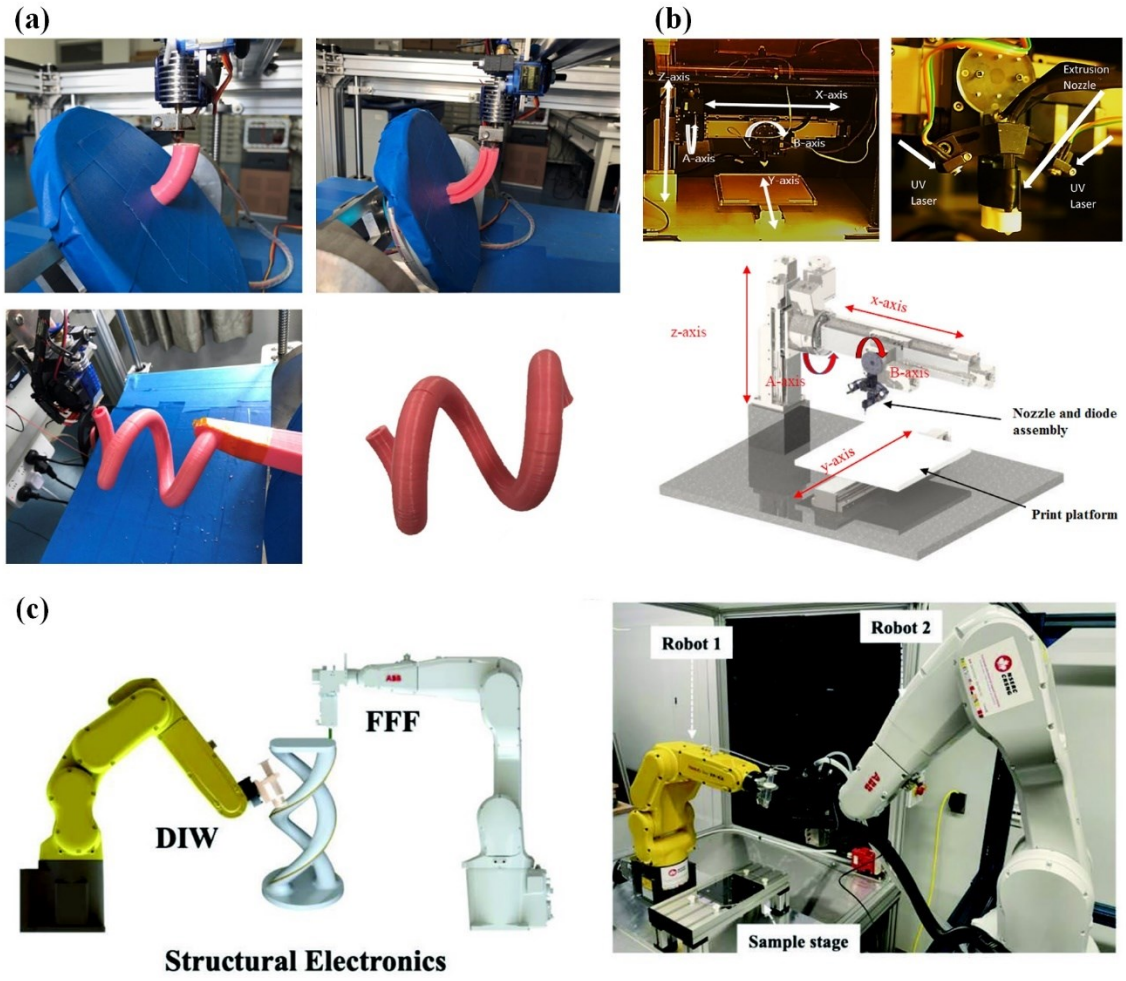

Figure 2.2. **(a) The 5-axis 3D printing system based on the rotation of the print plate. Reproduced with permission [52]. Copyright 2019, Robotics and Computer-Integrated Manufacturing. (b) The 5-axis 3D printing system by adding rotation to the printing nozzle. Reproduced with permission [54]. Copyright 2018, Additive Manufacturing. (c) The 6-axis robotic arm-based 3D printing system [56].**

2.1.2. 3D Printing Materials

The printable materials vary based on the AM process such that material types are divided into powder, sheet, wire, and liquid forms. Specifically, for FDM as the focus of the research, the printable materials are as follows [60]:

- Acrylonitrile Butadiene Styrene (ABS)
- Polycarbonate
- PC/ABS Blend
- Polylactic Acid (PLA)
- Polyetherimide (PEI)
- Polymer bound
- Polyetheretherkeytone (PEEK)
- Thermoplastic polyurethane (TPU)
- Chocolate

In the research, two main materials were considered: PLA and TPU. In the study of printing materials but not limited, the materials can be divided broadly into rigid and flexible materials based on its stiffness and shore hardness scale [61, 62, 63]. PLA filament used for the fabrication shows the following properties as follows [64]:

Table 2.1. Property of PLA Filament for FDM 3D Printers

Properties	Values	References
Density [g/cc]	1.24	[65, 66]
Glass transition temperature (T_g) [°C]	53 – 64	[67]
Crystalline melting temperature (T_m) [°C]	145 – 186 150 – 155	[67, 68]
Melt processing temperature [°C]	> 185 – 190	[69]
Tensile strength [MPa]	29.9 – 46.3	[70]
Hardness (Shore D)	48 – 87	[71]

Furthermore, the TPU filament is divided into different types based on its shore hardness scale such as 80A, 85A, 90A, 95A, 64D, and 72D [72]. Typically, shore A hardness scale measures the hardness of flexible mold rubbers that range in hardness from very soft and flexible, to medium and somewhat flexible material. On the other hand, shore D hardness scale measures the hardness of hard rubbers, semi-rigid plastics and hard plastics [73]. In this study specifically, the TPU-85A material was considered due to its challenges with fabrication process. The mechanical property of TPU-85A filament is as follows:

Table 2.2. Property of TPU Filament for FDM 3D Printers

Properties	Values	References
Density [g/cc]	1.11	[74, 75]
Glass transition temperature (T_g) [°C]	55 – 85	[76, 77]
Crystalline melting temperature (T_m) [°C]	163.5 – 190	[78]
Melt processing temperature [°C]	> 200 – 216	[78, 79]
Tensile modulus [MPa]	12	[72, 80]
Hardness (Shore A)	85	[71]

Furthermore, the Young's modulus or stiffness of different materials can be explained with the graph shown in Figure 2.3 below. Based on the Table 2.1 and Table 2.2 above, PLA shows lower flexibility in terms of its strength and hardness scale. Also, the PLA filament is classified under shore D scale and TPU lies under shore A scale. In this study, the representation of rigid material is selected PLA and flexible material to be TPU-85A [81, 82].

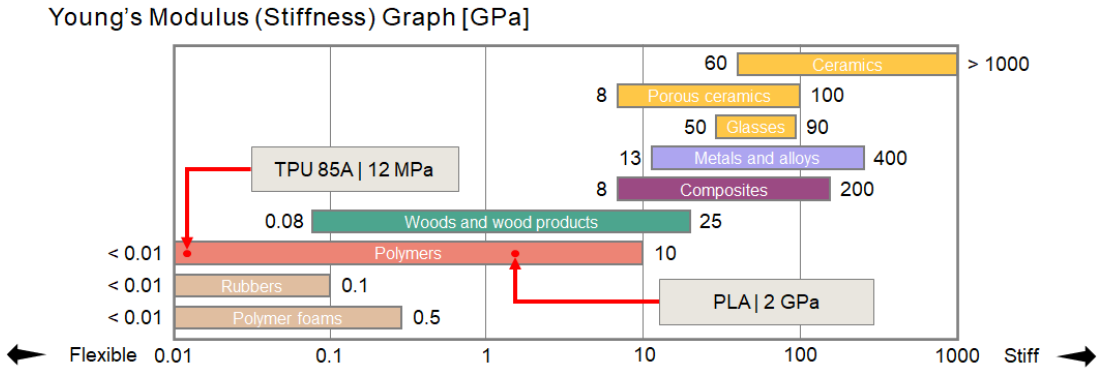

Figure 2.3. The Young's Modulus (Stiffness) graphical representation of different materials.

2.1.3. Challenges in 3D Printing with Flexible Materials

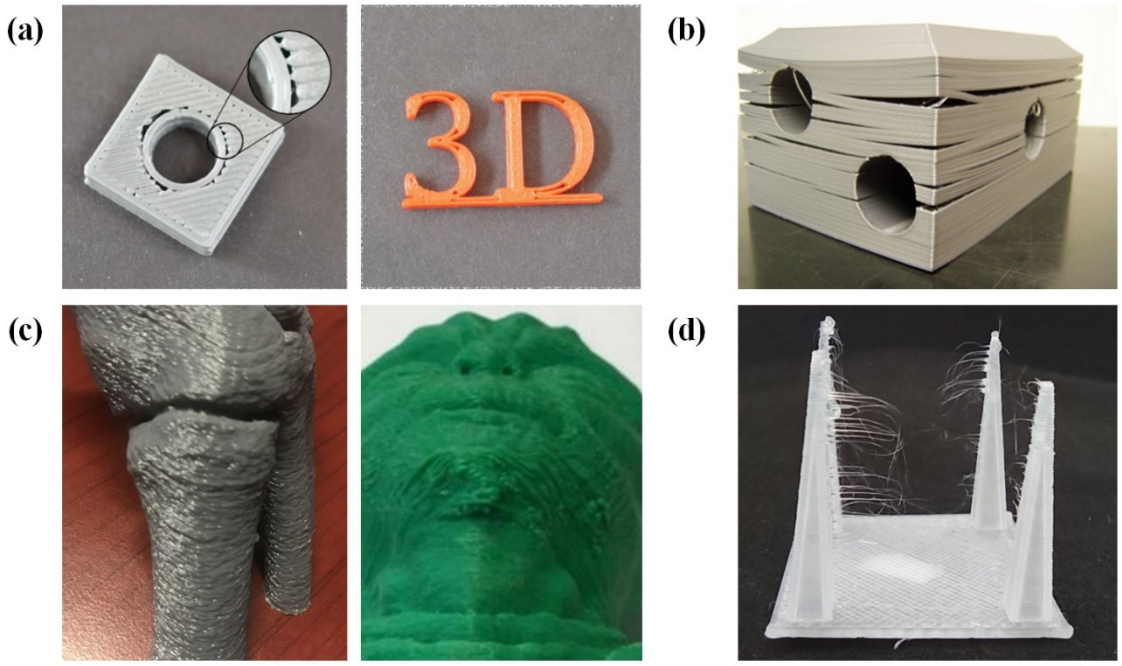

Figure 2.4. The common quality issues found in FDM process (a) Gaps in between layers. Reproduced with permission [83]. Copyright 2019, International Journal for Interactive Design and Manufacturing. (b) Layer delamination. Reproduced with permission [84]. Copyright 2016, Springer eBook. (c) Blobs and Zits [85, 86] (d) Stringing issues [87]

As briefly mentioned above, the 3D printing process with flexible material has critical challenges with its printability and printing quality [88, 89]. Some of the common print quality issue found in the 3D printing process are gaps in between layers [90, 91], layer separations or delamination [92], blobs and zits [93], and stringing [94] as shown in Figure 2.4. Furthermore, the printability issue is addressed by mainly two reasons: nozzle clogging [95] and filament buckling [96]. The nozzle clogging is one of the most significant errors that occur in the printing, and its occurrence has three reasons: presence of external particles on the filament, filament carbonization due to burning, and absence of place for extrusion [97]. Some studies have been conducted to detect the clogging or potentially clogging status on the FDM printers using captive detector that can operate inside high temperature [98]. The filament buckling issue is more common for flexible materials due to two mains reasons, high PE flexibility [99] and low column strength [100].

2.2. Artificial Intelligence (AI)

One of the methods to recover the disadvantages of the commercial FDM printing techniques is to control printing parameters manually for defects or restart the printing process. Plenty of study have been conducted to predict the performance of the printers by monitoring specific parameters such as temperatures [101] and nozzle conditions [102]. However, these methods require accurate mathematical and physical models representation to the specific issues. The difficulty of developing such system dramatically increase due to complexity of the printing processes. Unlike the indirect monitoring methods, the operators usually monitor the printing process to distinguish defects and control printing parameters manually [103]. As the appearance of the printed parts play a great role in determining the occurrence of defects, the operator's manual control is one of the simplest ways to enhance the quality of the 3D printing process.

However, due to the slow fabrication speed of commercial FDMs, different research have been studied as mentioned such as increasing the degree of freedom of motion to minimize support structures. Even with minimized or no supports are printed for the 3D model, the fabrication speed of 3D printers is still a known obstacle of entering the mass-production era [104, 105, 106]. As so, it is not possible for the operators to just wait by the printer to monitor the process in real-time.

For solutions to minimize human effort, the study on developing computer vision system-based quality control of the 3D printing process have been investigated. Some of the study focuses on the defects found in the part geometry [107, 108] or infill patterns [109, 110, 111]. The presented methods require the process to be paused to recreate 3D model of the printed parts with its point cloud which is time-consuming and computationally heavy. The further investigation for the current development of human-free quality control of the 3D printing process have been completed. The studies include both real and non-real-time parameter control using different types of AIs for different printing issues.

2.2.1. AI Categorization

The intelligent systems that offer AI capabilities often rely on machine learning algorithms. Often the machine learning and deep learning algorithms are considered into two distinct but similar features [112]. The machine learning describes the system learning

from the problem-specific training data to automate the analytical model building and solving processes [113]. The deep learning is classified as the subset of machine learning where the term deep refers to the number of layers in the neural networks [114, 115] as shown in the Venn diagram in Figure 2.5.

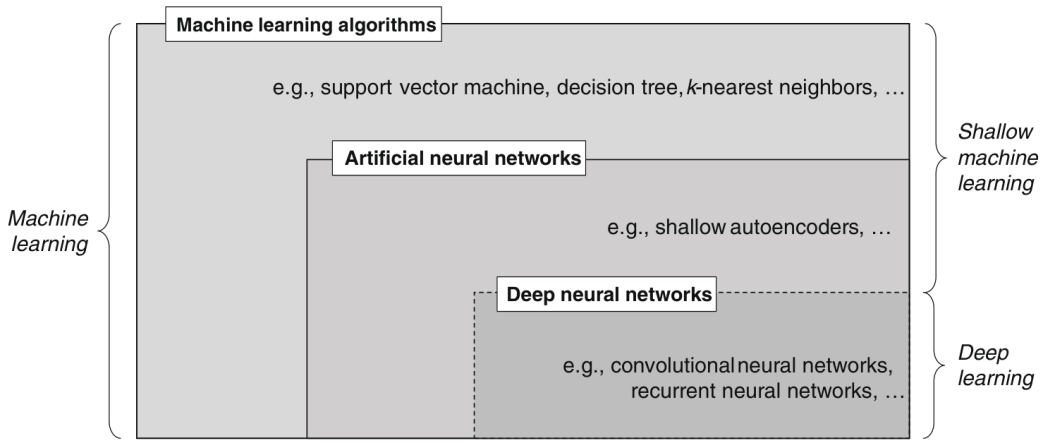

Figure 2.5. The Venn diagram showing the hierarchical relationship between machine learning algorithms, artificial neural networks, and deep neural networks [116]

The major machine learning achievement was Support Vector Machines (SVM) proposed by Vapnik and Cortes in 1995 [117] where this was the time isolating machine learning group into SVM or Neural Networks (NN) studies. Different classifiers were developed such as Adaboost by Vapnik and Cortes in 1997 [118] and Random Forests by Breiman in 2001 (RF) [119] which are used as a basis of classification model. Near today with opening to the new era of NN, deep learning, the different algorithm models were developed such as Linear Classifier [120], Logistic Regression [121], Naïve Bayes (NB) [122], Bayesian Network [123], Random Forest [124], Bootstrapped Aggregation (Bagging) [125], k-Nearest Neighbour (k-NN) [126] and Artificial Neural Network (ANN) [127]. The applications of machine learning are divided into different domains, computer vision, prediction, semantic analysis, natural language processing and information retrieval [114]. As the research focuses on the computer vision system, the further investigation was completed for the computer vision system. The computer vision system consists of object recognition and detection [128, 129].

The deep learning, as a subset of machine learning is a neural network with large number of layers and parameters (complex models). In short, deep learning employs a

sequence of multiple non-linear layers for extracting and transforming features [130]. The complexity of the features increase as the layer number increases meaning that the deep learning is able to analyze and extract the useful information from the data collected from different sources [131]. Specifically, different neural networks designs were developed such as Restricted Boltzmann Machine (RBM), the generative stochastic ANN [132], Recurrent Neural Networks (RNN), NN capable of recovering the stored pattern [133], Bidirectional Recurrent Neural Networks (BRNN), capable of training simultaneously in positive and negative time direction [134], Long Short-Term Memory (LSTM), consists of multiplicative gate units learning to open and close access to the constant error flow [135], and Convolutional Neural Networks (CNN), suitable for image detection and classification [136].

Furthermore, based on the problem and dataset, the machine learning algorithms can be classified into three categories: supervised learning, unsupervised learning, and reinforcement learning. Many applications use supervised learning such as stock market forecast system [137], understanding customer perception and needs [138, 139], etc. Also, reinforcement learning for the optimal control [140] or unsupervised web applications for microservices [141]. More specifically, the three types can be divided based on the knowledge of the input data.

The supervised learning requires a training dataset to include examples of the classes or known as labelled data [142]. An example could be the prediction of output for the provided input based on the provided specific relationship between input and output. The unsupervised learning on the other hand, does not require pre-existing labelled data [143]. In the case of unsupervised learning, the training data only contains input without known output requiring the algorithm to detect patterns by finding the structural information of interest from the dataset. The reinforcement learning system describes the current state of the system instead of dividing the input and output [144]. The system experiences process of achieving goal by trial-and-error process.

2.2.2. AI in 3D Printing

The study on the application using AI to enhance 3D printing processes have been conducted with different types of AI and AM processes. Different types of AIs such as Transfer Support Vector Machine (TSVM), Conditional Adversarial Network (CAN), Naïve

Bayes Classifier and J48 Decision Trees (NBC & J48), Bayesian Networks (BN), Filter bank and SVM in FDM, Electron-Beam Melting (EBM), Laser Powder Bed Fusion (LPBF), Selective Laser Melting (SLM), and SLA AM devices.

Guo et al. [145] applied TSVM to FDM for the fault diagnosis approach for the conventional delta 3D printer, type of FDM. The new learning method, transfer component analysis (TCA) [146] was utilized to extract cross-domain and massive unlabelled data from the target. The fault classification of 83.79% was achieved to improve the 3D printer fault diagnosis process. Li et al. [147] utilized CAN to commercial FFF printers to reduce inconsistency and 3D geometrical inaccuracies in the fabrication process as shown in Figure 2.6a. The developed system showed accuracy of 44.4%, 87.6%, and 99.2% for data within ±0.05mm, ±0.10mm, and ±0.15mm correspondingly. Wu et al. [110] developed the integration between NBC and J48 to classify defects developed on the surface of printed layers as shown in Figure 2.6b through FDM. The accuracy of the developed algorithm showed 95.51% for two-class classification, with and without defects. Bacha et al. [148] introduced the combination of BN theory and data acquisition techniques for fault diagnosis for the FDM. The system was developed with two cases with variations of a parameter, maximum number of parents in the calculation, and the classification results were found to be 92.56% and 98.18% for the parameter being 1 and 3 accordingly. Scime et al. [149] introduced in-situ monitoring and analysis for LPBF process using Filter bank with computer vision system. The overall classification results showed 98% overall with 95% accuracy among anomalies, 100% accuracy for anomaly-free regions, and 89% anomaly identification accuracy. Zhang et al. [150] proposed SVM to identify anomalies with LPBF printing process using high speed camera as shown in Figure 2.6c. The features of different objects such as melt pool, plume and spatter were investigated, and the classification accuracy showed 90.1%.

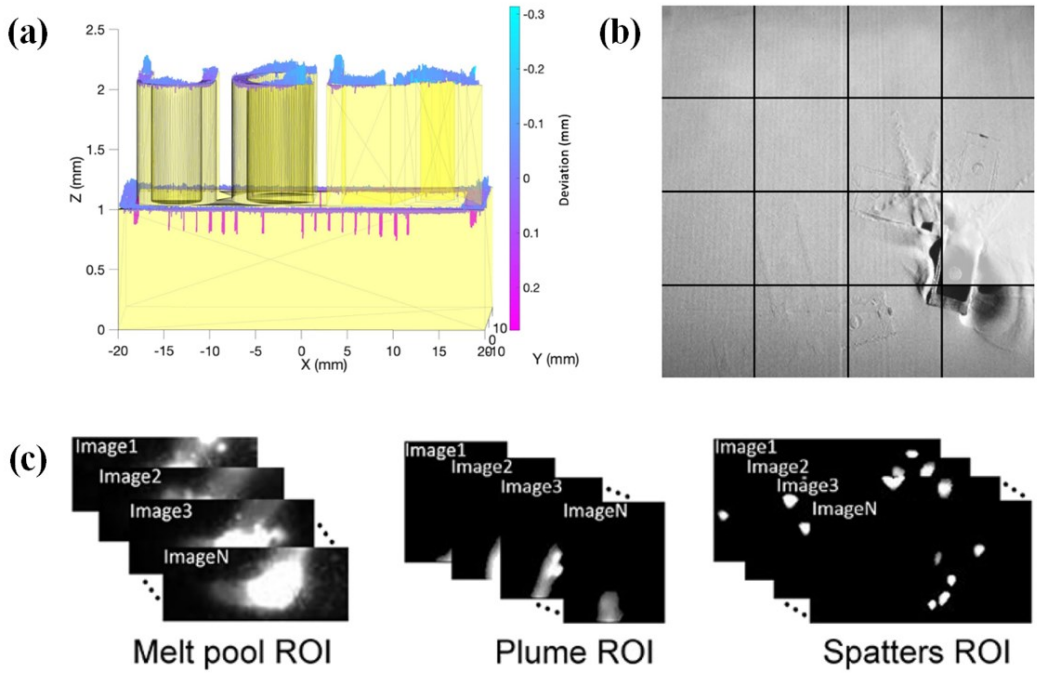

Figure 2.6. **(a) The illustration of the inconsistency and inaccuracies in 3D geometric structure. Reproduced with permission [147]. Copyright 2021, Additive Manufacturing. (b) The example of anomalies on the surface of LPBF process. Reproduced with permission [149]. Copyright 2018, Additive Manufacturing. (c) The Regions of Interest (ROIs) of melt pool, plume, and spatters for the LPBF. Reproduced with permission [150]. Copyright 2018, Materials & Design.**

2.2.3. Convolutional Neural Networks (CNN)

The different types of deep learning or machine learning algorithms were previously studied for the quality control of different, CNN shows higher accuracies in comparison to other classification methods [150]. Quite a few numbers of studies were conducted for FDM/FFF, LPBF, SLA devices. Lee et al. [151] investigated the effect of flowrates on the printed model developed fault detection and flowrate correction algorithms for FDM printers as shown in Figure 2.7a. By utilizing CNN, the system showed 99.99% classification accuracy and corrected underflow and overflow issues within two to eight layers of printing process; and allow the printer to print models showing similar mechanical properties at different initial flowrates. Jin et al. [152] focuses on identifying and correcting the flow-related issues as shown in Figure 2.7b with computer vision system mounted at the nozzle. The CNN model was designed for the identification and the accuracy of 98% was resulted showing the faster identification of faults than human.

Similarly, Khan et al. [153] investigated defects found in the infill layers of the FFF process as shown in Figure 2.7c with computer vision system mounted at the top of the FFF printer chassis. The CNN model was also created and the suitable accuracy of 84% was found using 50 number of epochs. Not only limited to FDM or FFF printers, Scime et al. [154] and Yuan et al. [155] investigated application of CNN to LPBF printing systems to autonomously detect processing defects (anomalies) in the fabrication process. The anomalies occurrence during the interaction between recoater at the overall classification accuracy of 97% and powder bed and track width measuring system with classification accuracy of 93% were developed accordingly. Khadilkar et al. [156] utilized CNN to predict stress distribution on the cured layer of the bottom-up SLA process-based models in real-time. The CNN resulted 5.6% prediction error with input data of sliced layer view of the CAD model.

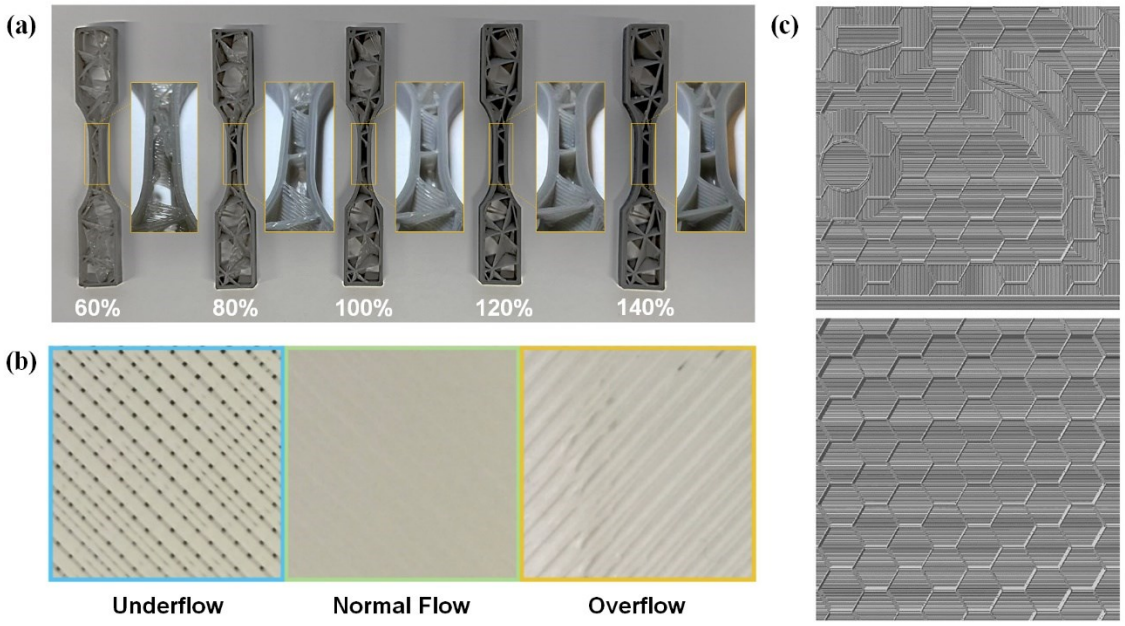

Figure 2.7. (a) The printed ASTM D638 Type V models at different flowrates [151] (b) The three types of flow-based conditions of FDM. Reproduced with permission [152]. Copyright 2019, Manufacturing Letters. (c) The surface defects found in the infill layer from the FDM process. Reproduced with permission [153]. Copyright 2021, Materials Today: Proceedings.

Chapter 3. Development of Rapid 3D Printing System

3.1. Hardware System

Prior to the initiation of the intelligent rapid 3D printing system development process, critical decisions had to be made regarding the hardware and software design specifications. This include, the selection of test specimen, selection of the printing parameters to be controlled, method of CNN design development, and experimental design. As mentioned above, the main scope of the research study is 1) to reduce stringing and blobs defects developed through the fabrication process 2) to sustain the mechanical properties of fabricated samples at the increased printing speed 3) to ensure the printability of the flexible material printing process.

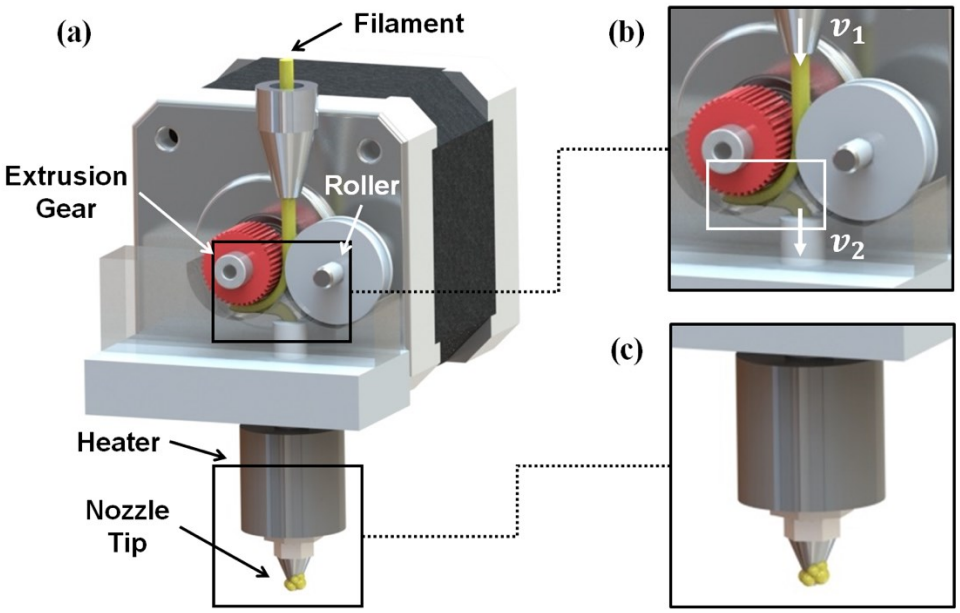

Figure 3.1. (a) The overview of the mechanical failure of FDM extruders (b) The graphical presentation of filament buckling phenomenon. (c) The graphical representation of blobs building around the nozzle tip.

As briefly mentioned above, the two main issues of the 3D printing process especially FDM is the defects and mechanical failure such as nozzle clogging or filament buckling issue. As shown in the Figure 3.1. Mainly the filament buckling shown in Figure

3.1b occurs when the filament extrusion rate is much lower than the filament feed rate ($v_2 << v_1$). To further investigate the reasons behind the filament buckling phenomenon, the loading conditions on the filament needs to be analyzed, and shown below is the Euler's critical loading condition [157]:

$$P_{cr} = \frac{\pi^2 EI}{L^2}$$

For the two materials PLA and TPU as shown in Table 2.1and Table 2.2, it is clear that the filament buckling phenomenon is more probable for flexible material TPU with its much lower modulus of elasticity (E) compared to rigid material PLA. Considering both conditions of filament buckling phenomenon, it shows the critical reason behind limited fabrication speed of flexible material. Furthermore, to find the critical speed limitation of the selected filament, the complex model was printed at different printing speed as shown in the Figure 3.2. The FDM printer (Formbot VIVEDINO T-Rex 3+) was used for all of fabrication process in the study. At the same printing speed setting of 30mm/s, TPU was not able to complete the printing process when operated without any intermediate parameter control as shown but hardly showed similar results at the half of printing speed as the printed model with PLA. The critical speed of interest in the study, therefore, was selected to be 15mm/s which is set as the basis for the performance test of the developed system.

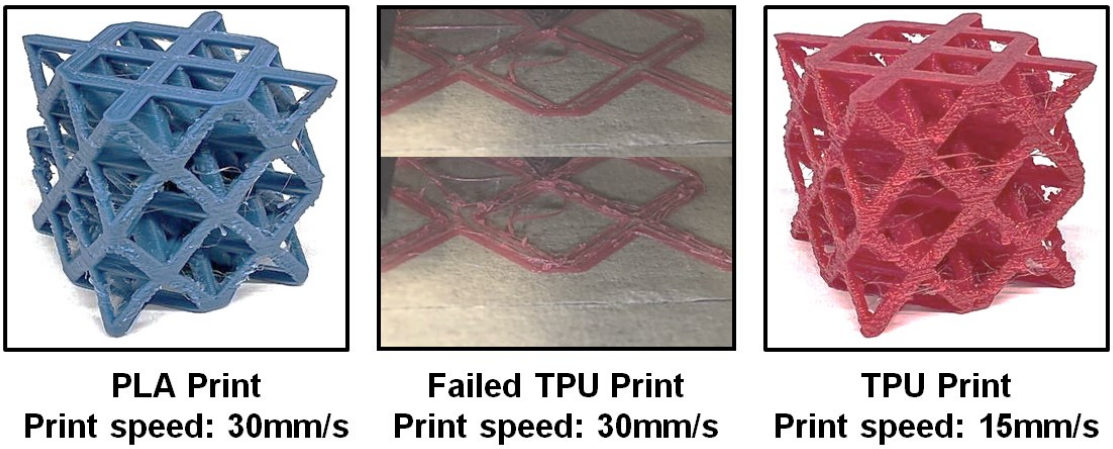

Figure 3.2. The comparison between the printing results of complex 1D strut-based Octet 2×2×2 model printed by PLA and TPU at different printing speed.

3.1.1. Testing Models

In the process of selecting the test specimen for the study, three criterions were considered: 1) compression test friendly model 2) complex structure for 3D printing process that can be fabricated without support structure 3) structures showing clear changes with different printing parameters. Among several miniaturized architectures, 3D periodic octet and 3D surface gyroid models have been selected as the test models where the octet is one of the most complex 1D strut-based structures and the surface gyroid is one of the most complex 2D sheet or curve-based structures [158, 159, 160, 161]. The octet was designed by developing a unit cell size of 15mm×15mm and eight cells were assembled to create 30mm×30mm×30mm structure, defined as Octet 2×2×2. The gyroid was designed based on the mathematical equation representation to create 30mm×30mm structure consists of 8-unit cells as well, defined as Gyroid 8 [162]. Developed structures are shown in the Figure 3.3.

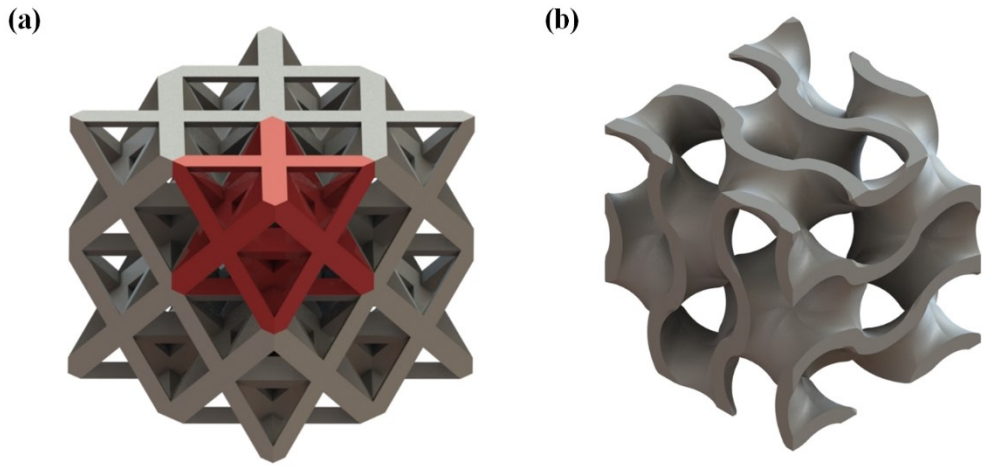

Figure 3.3. The CAD rendered image of developed test specimens (a) Octet 2×2×2 (b) Gyroid 8.

3.1.2. 3D Printing Parameters

To enhance the printing quality beyond proper calibration, several printing parameters can be modified during the printing process in real-time. These parameters include the print bed temperature, z-offset, flowrate, nozzle temperature, and print speed [163]. Adjusting these parameters can improve the adhesion, accuracy, and surface finish of the object being printed. The print bed temperature and z-offset generally only need to

be adjusted at the beginning of the process as they are the most effective parameter to ensure the print adhesion on the print bed. The z-offset is key to preventing nozzle grinding the print bed or printing on air due to incorrect settings. The effect of the flowrate on the printed parts has been investigated previously especially inspecting the effect of underflow and overflow issues and their results on the printed parts [110, 164, 165]. The nozzle temperature does not show a clear visual effect on the printed part in comparison to flowrate, but it has more impact on the printability. With incorrect nozzle temperature, the extrusion process can fail as the filament is not able to melt into a liquid form causing the filament buckling issue or blobs can build on the nozzle tip causing carbonization inside and outside of the nozzle in the long run [165, 166, 167].

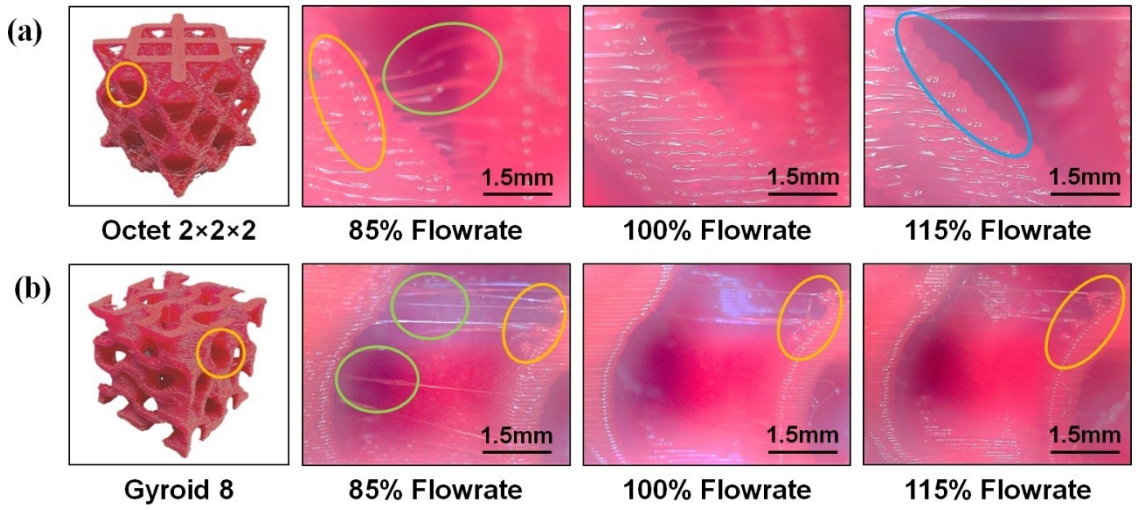

Figure 3.4. The visual defects of developed on the test specimens (a) Octet 2×2×2 (b) Gyroid 8 at different flowrate settings.

For the selection of control parameters, flowrate and nozzle temperature were selected and tested. Under the print speed of 15mm/s, the flowrate was tested at 85%, 100% and 115% at constant temperature as 230°C. Then temperature was varied for the printing test at 225°C, 235°C, and 245°C for constant flowrate as 100%. The printed models were visually analyzed, and a compression test was conducted to find a non-visual effect of the parameters. The visual test result of octet and gyroid with varying flowrate are shown in the Figure 3.4. Low flowrate causes gaps in between layers due to insufficient amount of extruded material and stringing between the structures. The high flowrate causes collapsing of the layers due to an excessive amount of extruded material and results in curved edges instead of straight edges.

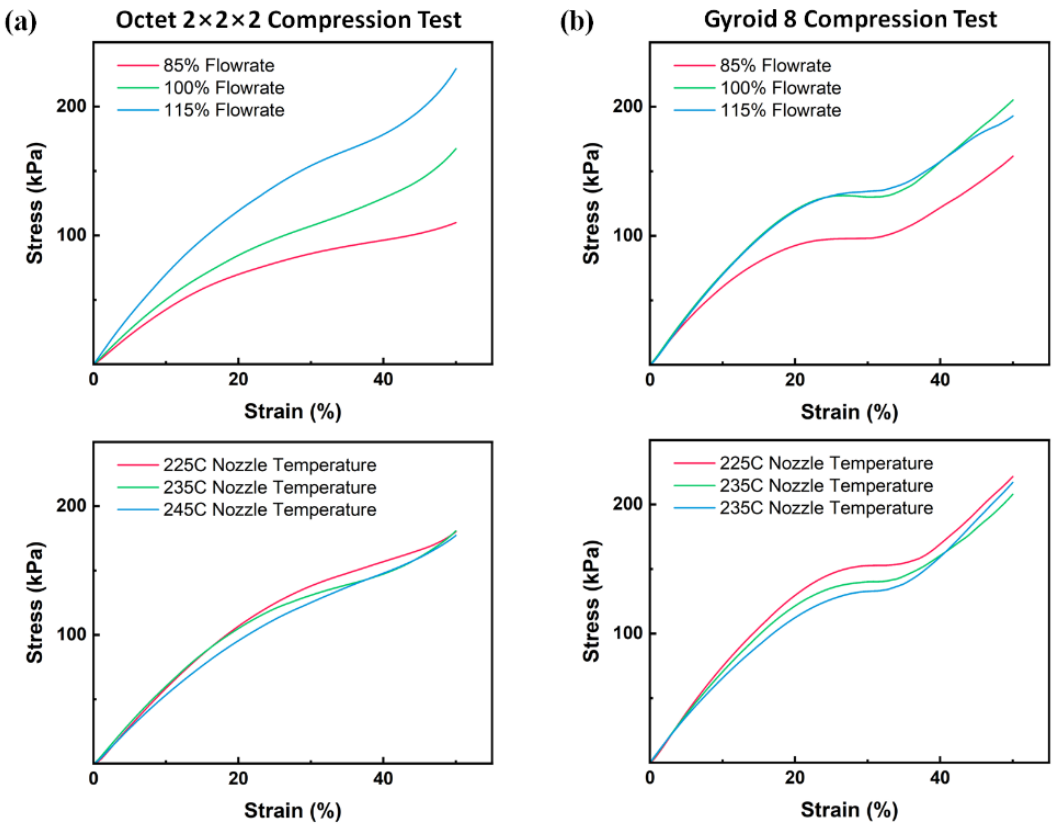

Figure 3.5. The stress-strain curve representation of the compression testing results of (a) Octet 2×2×2 (b) Gyroid 8 at varying flowrate and nozzle temperature.

Figure 3.5 show the compression test results of the octet and gyroid models with varying flowrate and nozzle temperature settings. The result shows that the octet shows an average of 2.436% strength change per flowrate percentage change, and the gyroid shows an average of 1.673% strength change per flowrate percentage change. However, varying nozzle temperatures showed little to no structural changes as well as compressive strength. Gibson and Ashby et al. demonstrate the relationship between the mechanical properties of cellular structure and the relative density such as stress and strain [168]. The relationships known as the Gibson-Ashby model are represented with the following equations below:

$$\frac{E_L}{E_S} = C_1 \left(\frac{\rho_L}{\rho_S}\right)^n$$

$$\frac{\sigma_L}{\sigma_S} = C_2 \left(\frac{\rho_L}{\rho_S}\right)^n$$

where E, ρ, and σ represent the elastic modulus, density, and yield strength respectively; cellular structures denoted as L and base solid model denoted as S. Shown in Figure 3.6 is the Gibson and Ashby plot of relative compressive strength in respect to relative weight density. Based on the test of five printed samples, the plot was completed, and one interesting phenomenon was found. From the underflow case, the increased flowrate enhances the performance of both models closer to the ideal bending-dominated behaviour. On the other hand, from the limit of 100% flowrate, the increased flowrate rather decreases the performance as the excessive amount of extruded filament increases the overall weight of the object without enhancing its performance. As so, flowrate has been selected as a primary parameter to control for the in-situ correction system, but the nozzle temperature is set to be a secondary parameter as it is a key parameter to ensure the printability of flexible material.

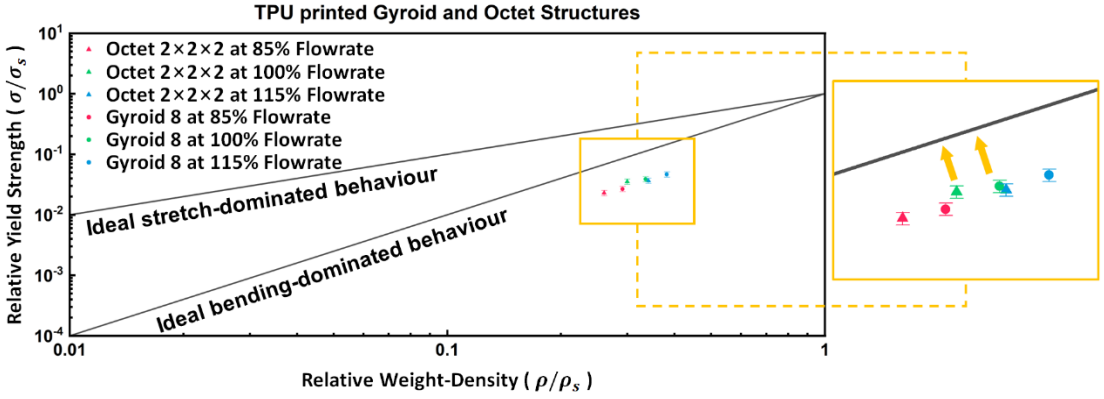

Figure 3.6. The Gibson-Ashby model representation of the relative yield strength vs relative weight-density of two specimen at different flowrates.

3.2. System Workflow

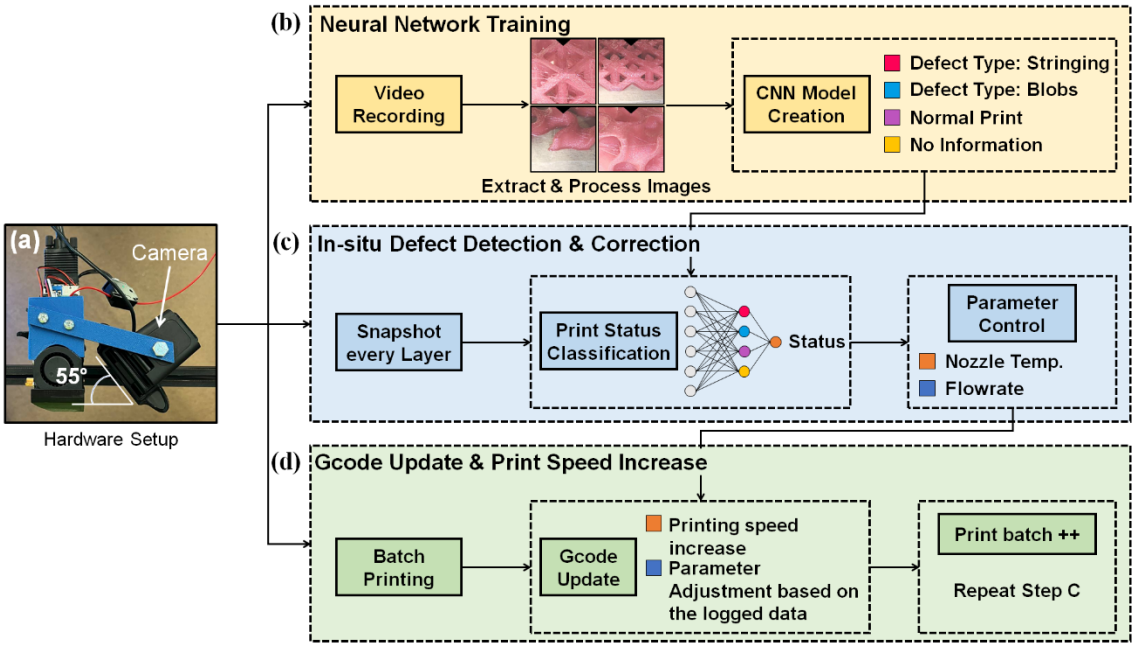

Figure 3.7. The system flowchart of rapid 3D printing system. (a) The hardware setup. (b) The neural network training process. (c) Defect correction process. (d) Rapid printing system process.

The development of the defect detection and correction system is divided into three parts: 1) neural network training, 2) in-situ control system, and 3) print speed optimization. As the machine learning-based defect detection system is selected for the method of the classification algorithm, the image acquisition system is critical. The camera (Logitech C270) used in this study was strategically mounted at a 55-degree angle using a 3D printed special mount as shown in Figure 3.7a. This angle was chosen based on the optimal viewpoint for the 3D printed objects, allowing the acquisition of all important information from the image [169]. The neural network training is the first step in developing the defect detection and correction system where the properly trained model is crucial for the enhanced performance. This step involves collecting images of known good and defective models, and it was completed by extracting images frame by frame from the recorded video of the printing process as shown in Figure 3.7b. Based on the pre-trained CNN model, the in-situ control system was developed as shown in Figure 3.7c. The control system monitors the 3D printing process in real-time and controls two parameters, flowrate and nozzle temperature as needed to ensure printability and to correct defects. The

captured images are processed, and the pre-trained CNN model classifies the adjustment that needs to be made. The final step of the system involves print speed optimization where the print speed is increased every batch of print along with the applied correction as shown in Figure 3.7d. The printability and quality control are completed from the previous step, but the print speed limitation is still a problem with the printing of flexible materials. The developed speed optimization system logs the correction data and applies it to the g-code directly and the updated g-code is used to print the next batch.

3.3. Design of CNN Model

CNN training is one of the supervised learning processes where the input images are classified by the operator. In this study, four different defect types were classified as 1) stringing defects, 2) blob defects, 3) normal printing, and 4) no information. The class of no information is defined for the first 30 and last 10 layers of the print as it contains no useful information and shows low flowrate and nozzle temperature impact to the print quality. In the development of a convolutional neural network (CNN) model, various hyperparameters can be adjusted to improve the accuracy of the classification results. These include the kernel size and filter, convolutional layers, epoch, activation functions, and optimizers.

The kernel size is a parameter that determines the size of the filters used in the convolutional layer. The kernel filter is a small matrix that slides across the input image, performing a mathematical operation at each location. The kernel size has a direct impact on the number of features extracted from the input image, with larger kernel sizes extracting more features. However, it is also important to note that a larger kernel size increases the total number of parameters in the CNN model, potentially leading to overfitting.

The convolutional layer is responsible for analyzing the input image and extracting features from it. The size of the layers in the CNN development process is determined by the number of filters used for the feature extraction process from the input image. Each filter in the convolutional layer is applied to the input image with the kernel filter across the image. A larger number of filters in the convolutional layer extracts more features, but it also increases the total number of parameters in the model, which can lead to overfitting.

The epoch is the number of times the entire dataset is passed through the CNN network during the training process. Each epoch is a complete iteration of the training process, where the calculated weights of the network are updated based on the errors. A larger epoch size allows for more training, which can lead to better performance. However, it also increases training time and can lead to overfitting.

The activation function is the mathematical function applied to the output of each neuron to determine the output. The output of the neuron, known as the activation, is used as the input for the next layer in the network. It also introduces non-linearity to the neural network, allowing it to learn complex patterns from the input image data. Different types of activation functions, such as ReLU (Rectified Linear Unit), Sigmoid, Tanh, and more, have different characteristics. The selection of the activation function depends on the specific problem or task and personal preference.

The optimizer is the algorithm used to adjust the weights of the network to minimize the loss function. The loss function is a measure of the network's performance on the training dataset. The main objective of the optimizer is to find the set of weights that minimizes the loss function, leading to the best performance of the network. Different types of optimizers, such as SGD (Stochastic Gradient Descent), Adam, Adagrad, and more, are available. Similar to the activation function, the best optimizer for a particular problem depends on the specific architecture of the network and the dataset.

For the specific development process for the system, different variations of hyperparameters were considered as shown in Table 3.1.

Table 3.1. CNN Hyperparameter Variations

Kernels Setup (K1 – K4*)	16-3 | 32-3 | 256-3 | Avg. Pool 32-3 | 64-3 | 256-3 | Max. Pool 64-3 | 128-3 | 256-3 | Max. Pool 512-1 | Glob. Avg. Pool	16-5 | 32-3 | 256-5 | Avg. Pool 32-5 | 64-3 | 256-3 | Max. Pool 64-5 | 128-3 | 256-1 | Max. Pool 512-1 | Glob. Avg. Pool
	16-3 | 32-3 | 64-3 | 512-3 | Avg. Pool 32-3 | 64-3 | 128-3 | 512-3 | Max. Pool 64-3 | 128-3 | 256-3 | 512-3 | Max. Pool 1024-1 | Glob. Max. Pool	16-3 | 32-3 | 64-3 | 512-5 | Avg. Pool 32-3 | 64-3 | 128-3 | 512-3 | Max. Pool 64-3 | 128-3 | 256-3 | 512-1 | Max. Pool 1024-1 | Glob. Max. Pool
Activations Function (A1 – A6*)	Relu	Sigmoid Softmax
	Softsign	Tanh Selu
Optimizer (O1 & O2*)	Adam	SGD
Optimizer Learning Rate	0.0001 incremental	

3.4. Data Processing and Parameter Controls

The overall system consists of two computing devices, PC and Raspberry Pi 3+ and FDM printer. The USB serial connection was established between Raspberry Pi and FDM printer for the parameter control process while PC and Raspberry Pi was connected over-the-internet to perform specific communications. The design and programming of the system was implemented using Python programming language and CNN was developed by utilizing the Keras library. Furthermore, the virtual environment for the programming was established through Anaconda (Data Science Platform) where the programming itself was completed using PyCharm (Integrated Development Environment). The parameter control was completed by transferring the Gcode from Raspberry Pi to the 3D printer through USB serial communications. The slicing software for the developed model for printing, Cura was used with the specific settings shown in Table 3.2 below:

Table 3.2. The Slicer Software Setting

Nozzle size	0.4 mm
Layer height	0.2 mm
Wall thickness	0.8 mm
Infill	100% Density with Lines Pattern
Initial Printing Temperature	228 – 230°C
Retraction	Disabled
Print Speed	15 mm/s
Support Structure	Disabled
Build Plate Adhesion Support	Disabled

Different types of data were analyzed and used for communication between devices such as the real-time acquired image data, CNN classification results, and parameter control commands. The developed computer vision system provides 720-pixel image quality at 30 frames per second, and sufficient time delay was required to stabilize the extruder head for the image capturing process. The capturing process was completed at a fixed location layer-by-layer providing more consistent dataset for the CNN model. For the stabilization time 125ms was allocated in the image capturing process. In addition to the stabilization time, LED strip was mounted around the nozzle to allow consistent lighting and reduce shadows which possibly eliminates valuable information from the collected images.

During the training process, the camera records the printing process as a time-lapse video format via an open-source 3D printer interface called Octoprint. After recording, the frames are extracted from the video as images and classified before uploading to the CNN model. After the training completion of the CNN model, the image acquisition system was setup where it includes image transfer and processing. Following the image acquisition process, the several steps are designed to transform the raw data into CNN model favourable dataset. To minimize size of the raw data, the images were captured at 480 × 640 pixels size which is again reduced to 300 × 300 pixels. The smaller dataset does not only reduce the image transfer time, but it also reduces CNN classification processing time as well. Moreover, the CNN reliance on the colour information needed to be eliminated to increase the accuracy of the model and create robust classification system capable of identifying different types of defects regardless of the filament colour. The simple solution for the issue was to apply greyscale to the image data which had additional benefit of reducing the data size. For the final data processing

step, digital black bars were added to cover nozzle and heat core to reduce confusion on the CNN model.

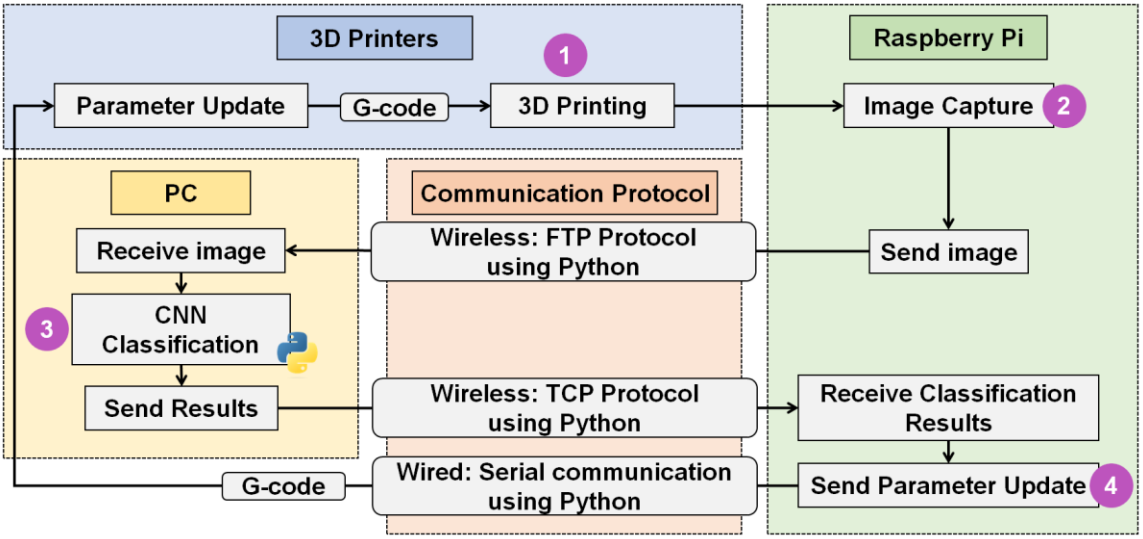

Figure 3.8. The system data process map. The data collected during the 3D printing process every layer is sent to PC through Raspberry Pi for the defect classification process, then sent back to Raspberry Pi for parameter control process.

As shown in the Figure 3.8, the original image was taken by Raspberry Pi then transferred to PC through FTP protocol for the image processing and classification function. After the CNN classification, the identification representation code for different defect class was then sent back to Raspberry Pi through TCP protocol to perform parameter control on the printer. All data processing was completed using Python programming language.

Based on the selected printing parameters, the control system was designed. Prior to the development of the control system, the minimum and maximum allowed parameters needed to be selected. Extrusion test was performed at different parameter settings and the results of the extrusion test is as shown in Table 3.3 below:

Table 3.3. Minimum and Maximum Allowed Printing Parameters.

Nozzle Temperature (°C)	Flowrate Allowed (% with basis from 15mm/s)
225 – 227	85 – 97
228 – 229	85 – 108
230 – 233	85 – 115
> 233	Filament Carbonization

The test results shows that the maximum allowed nozzle temperature is 233°C with minimum required temperature of 225°C to allow any extrusion. Furthermore, as the increased flowrate requires higher nozzle temperature, the control system was setup in a way that both parameters are carefully controlled simultaneously.

The control system was developed on the simple logic based on four classification results. The control system will

- Increase flowrate and nozzle temperature if the stringing defects are found
- Decrease flowrate and nozzle temperature if the blobs defects are found
- Keep the printing settings when the normal printing or no information class is identified

During the correction procedure, the minimum and maximum settings were always checked to avoid any printability issue occurrence during the quality control process. Furthermore, the maximum correction per layer (per classification process) was kept at 1% flowrate change as flexible materials are very sensitive to parameter changes.

3.5. Experimental Setup

The performance of the developed intelligent 3D printing system was tested using two main methods to confirm that the system met the objectives of the research study. These tests were crucial in determining the effectiveness of the developed system and its ability to achieve desired results. The first method was the defect control test. This test was designed to evaluate ability of the system to identify and correct any defects that may occur during the fabrication process. The system was expected to successfully detect and correct defects in real-time, ensuring the high quality of the printed model. The second method was the compression test. This test was designed to evaluate the mechanical strength and durability of the printed models. The models were subjected to increasing compression stress and the results were compared. The results of both the defect control and compression test were compared to the objectives of the research study.

3.5.1. Defect Control Test

The performance of the defect correction system was evaluated by monitoring the printing process. The primary goal of the testing was to investigate the efficiency and repeatability of the correction algorithm under different conditions. To accomplish this, the flowrate of the system was intentionally changed to the minimum (85%) and maximum (115%) at specific layers. The test was performed every 25th and 50th layer to repeat the process multiple times within a single printing process. One of the key features of the correction algorithm is its ability to correct the flowrate to the desired value within a certain number of layers. The system is set to determine the minimum required number of layers to reach the desired flowrate of 100% to be 15 layers.

In total, four types of tests were conducted for each model, three samples each providing a comprehensive evaluation of the performance of the correction system. The results of these tests will be used to improve the algorithm and ensure that the correction system works effectively under various conditions.

3.5.2. Compression Test

To further investigate and evaluate the performance of the newly developed system, various testing methods were evaluated, such as compression test, impact test, tensile test and others. Among the test specimens selected, Octet 2x2x2 and Gyroid 8, the compression test was deemed to be the most appropriate method. The stress-strain curve was used to compare the consistency of the models printed with a rapid process. The compression test was performed on five replicas, all of which were printed with the same settings and speed. The test was carried out using a Shimadzu EZ-LX Tester and was completed at a compression speed of 2mm/min. The slower compression test speed of 2mm/min was chosen for several reasons. Mainly, it provides a more accurate representation of the material's behavior under stress, giving a better understanding of its properties. A slower compression test also minimizes the risk of damage or failure on the test specimen, ensuring the reliability of the results. The slower compression test speed is more representative of real-world conditions and loading, making the results more applicable and relevant. The test took over 5 minutes to complete for each specimen, demonstrating the thoroughness and care taken in performing the tests.

Chapter 4. Results and Discussion

4.1. Defect Detection System

The final process of developing CNN model for defect detection involves classification accuracy testing. The aim was to ensure that the model can accurately identify defects from the provided three datasets: training, validation, and testing. To achieve this, over 50 different combinations of hyperparameters were considered during the development process. These hyperparameters are crucial for determining the structure and performance of the model, and a small change can cause accuracy variations over 70%. The combinations of hyperparameters included variations in kernel size and filter, convolutional layers, epoch, activation functions, and optimizers. Each combination was trained and evaluated for its performance on a validation set.

4.1.1. Design of Neural Networks

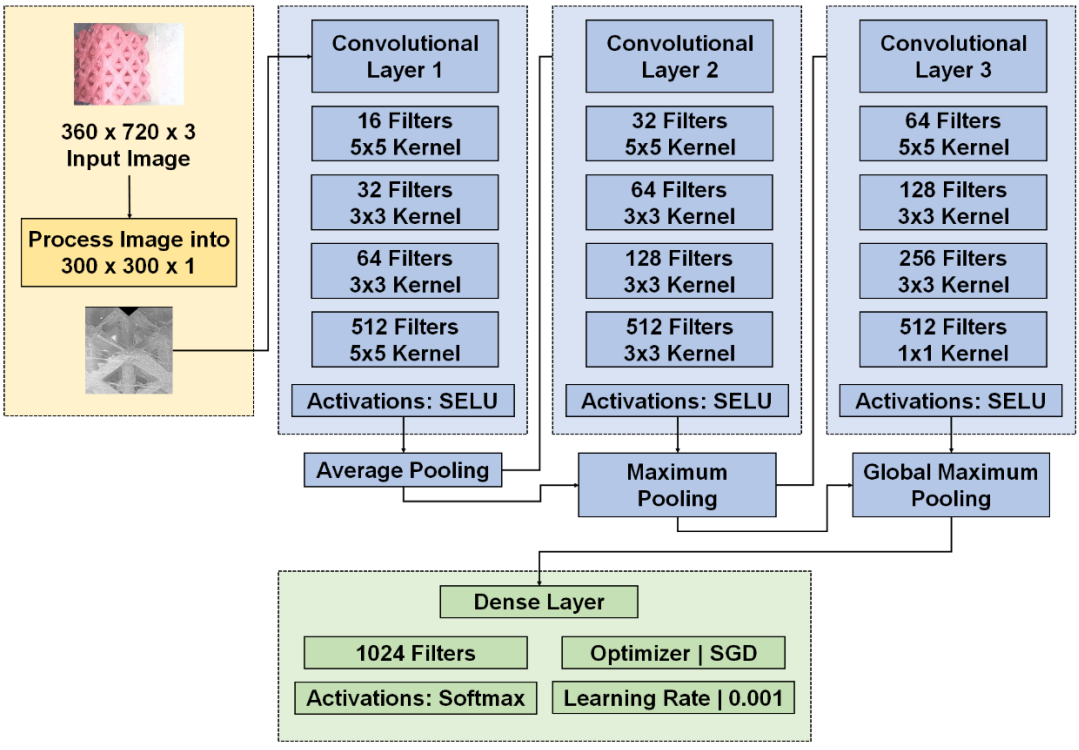

Figure 4.1. The overall flowchart of the developed CNN model. The model uses 300x300x1 (Greyscale) input image data and consists of three convolutional layers utilizing 1,024 filters in the dense layer.

After evaluating all the combinations, one particular set of hyperparameters was selected that showed the best performance. The selected combination showed a training accuracy of 98.97%, which means that the model was able to accurately identify defects in the data it was trained on 98.97% of the time. The validation accuracy was also measured, which was 97.82%. This indicates that the model was able to generalize well to new, unseen data and accurately detect defects in that data as well. The shown in the Figure 4.1 is the structure of developed CNN showing 98.97% training accuracy. As shown, the model consists of three convolutional layers and one dense layer with 1,024 filters. The key to the model is the connection between the pooling results from the previous pooling and the new pooling. This procedure is also known as Residual module and it provides higher accuracy [169].

4.1.2. Classification Accuracy

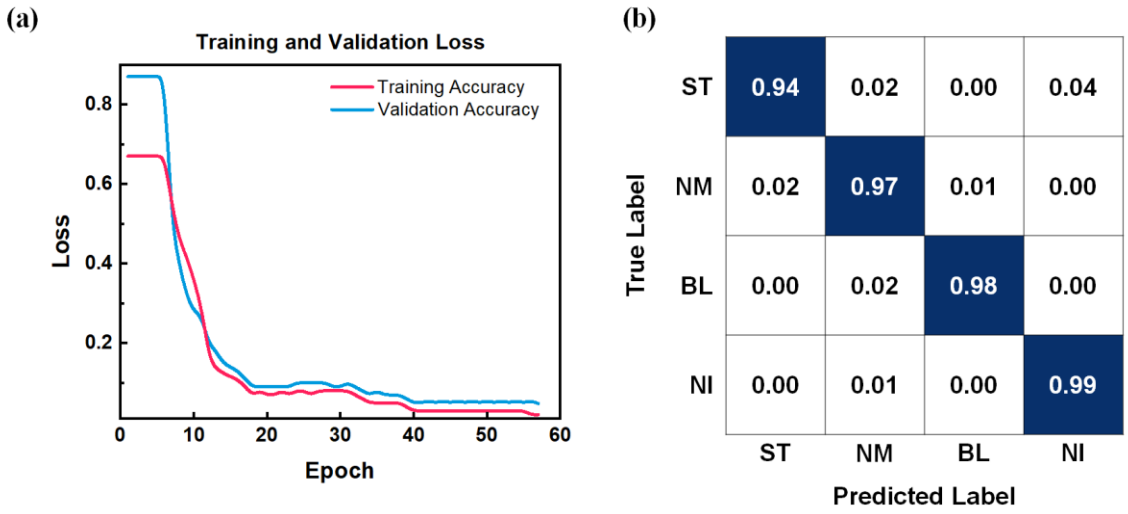

Figure 4.2. (a) The training and validation loss graph during the CNN model traning process (b) The confusion matrix representation of the developed CNN model.

The result of CNN is usually represented in terms of training and validation loss graph and confusion matrix [170, 171]. To further explain the performance of CNN, the prediction process needs to be explained. The CNN model identifies the input image based on the possibility chance of the defined classes. Then, the class with highest possibility chance is selected as a result. The training and validation loss graph is shown in the Figure 4.2a, and the final training accuracy was 98.97% with validation accuracy of

97.82%. This further proves that the overfitting issue was not present in the designed CNN model. The confusion matrix shown in the Figure 4.2b shows that the accuracy of classifying no information and blobs classes is relatively better than other classes. This is mainly because the images used does not provide enough resolution to detect all microscopic strings present in the sample. Specifically, the classification of the stringing defect is relatively less accuracy for the gyroid model compared to octet model.

4.2. Defect Control

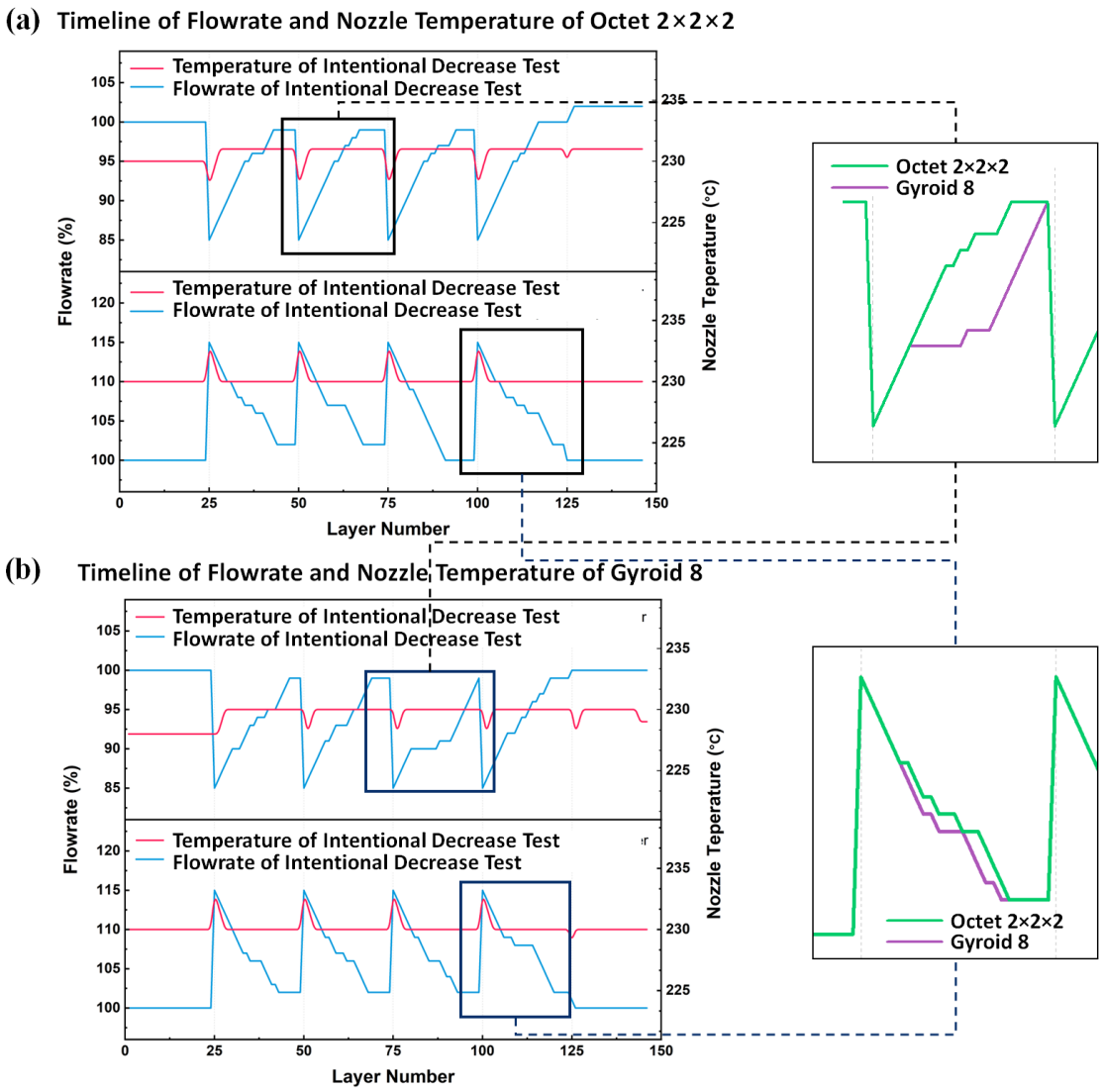

Figure 4.3. The correction timeline from the defect control test of (a) Octet 2×2×2 (b) Gyroid 8

The results of the performance test of the defect correction system were highly informative and provided valuable insights into the efficiency and repeatability of the correction algorithm as well as the effect of different printing styles. The correction timeline for the flowrate and nozzle temperature of gyroid in Figure 4.3a, and that of octet in Figure 4.3b. The test results were compared, intentional decrease in the yellow box and an intentional increase in the green box in the Figure 4.3. It is found that the underflow correction of the octet is more efficient than that of the gyroid model where the overflow correction is similar in both cases. The underflow error is detected based on the classification of stringing defects found in the print, and the difference in the detection accuracy comes from the structural difference between the two models.

4.2.1. Discontinuous vs Continuous Printing

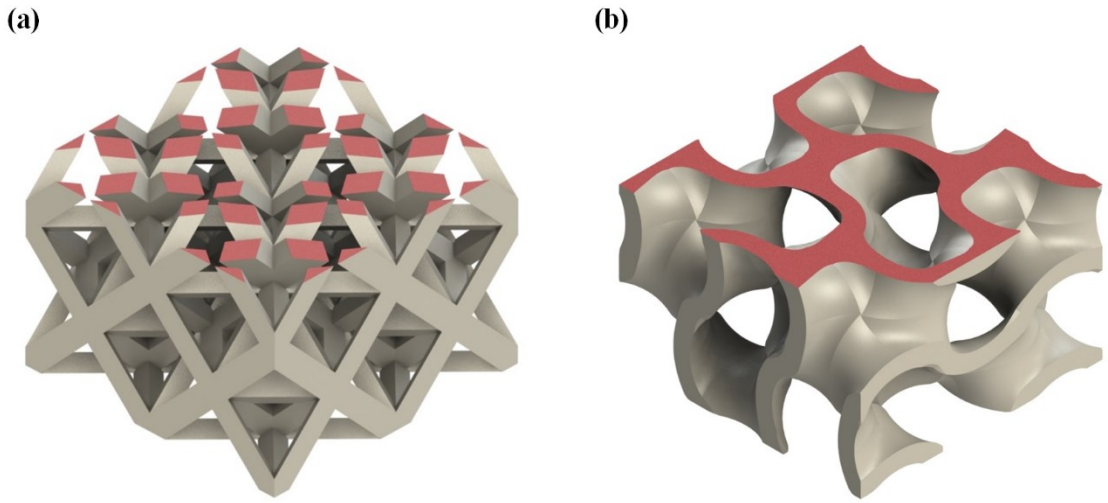

Figure 4.4. The printing layer view of (a) Octet 2×2×2 (b) Gyroid 8. The corresponding discontinuous and continuous layers are highlighted in red.

The research study compared the differences between continuous and discontinuous printing in the 3D printing process. The results of the study were shown in Figure 4.4, which provided a visual representation of the printing layer view of two different structures: Octet 2×2×2 and Gyroid 8. In the figure, a single layer (Layer 52 of 151) is highlighted in red, demonstrating a clear difference in printing styles.

The octet structure exhibits a discontinuous printing style characterized by distinct and separated structures. On the other hand, the gyroid structure can be described as having a continuous printing style, as seen in the sliced layer representation. This difference in printing style leads to different challenges in the printing process. For example, in the study, the discontinuous printing of octet was found to increase the occurrence of stringing defect, a common issue that arises during the nozzle travel between separated structures or when an underflow error is present. Considering the limitation of the hardware for collected images for the process, the system is not able to detect microscopic stringing defects in the print. The results of the study demonstrate the importance of considering the printing style in the 3D printing process. The discontinuous printing style of octet presents additional challenges compared to the continuous printing style of gyroid, which can impact the quality and consistency of the fabricated 3-dimensional objects. Understanding these differences is crucial in optimizing the printing process and ensuring high-quality results.

4.3. Rapid Printing Quality

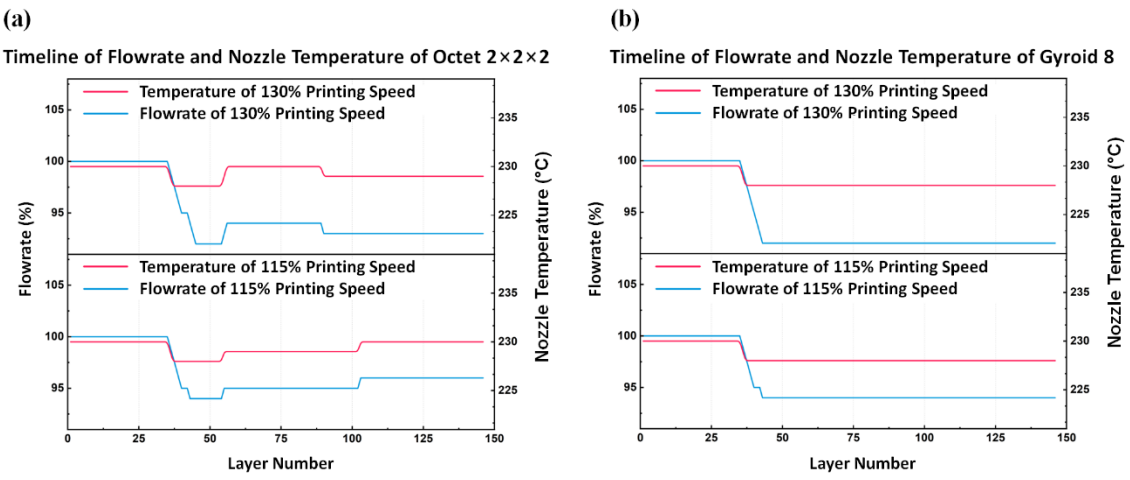

Figure 4.5. The correction timeline from the rapid printing test of (a) Octet 2×2×2 (b) Gyroid 8.

In the final part of the study, the focus was on maximizing the print speed while maintaining the printability and quality of the printed samples. To achieve this, the printing speed was incrementally increased, and the resulting models were evaluated for their mechanical properties with a compression test. The tests were conducted by increasing

the print speed by 15% and 30% and the results were compared to models printed at the standard print speed of 15mm/s. The goal was to adjust the printing parameters to save fabrication time without sacrificing the structural integrity. Figure 4.5 show the correction timeline of test models with 15% and 30% increased print speed, octet and gyroid respectively. In the slicing stage of the 3D printing process, the flowrate increases to maintain a consistent amount of filament extrusion and to ensure the printing process. However, as previously mentioned, the increase in flowrate increases the chances of the filament buckling failure occurrence with flexible materials. As so, the nozzle temperature control is crucial to increase the filament melting speed to reduce the stress applied on the nozzle with extrusion. For both cases of octet and gyroid, it is shown that the flowrate is generally decreased after around 30 layers of print with the detection of blobs which also ensures printability.

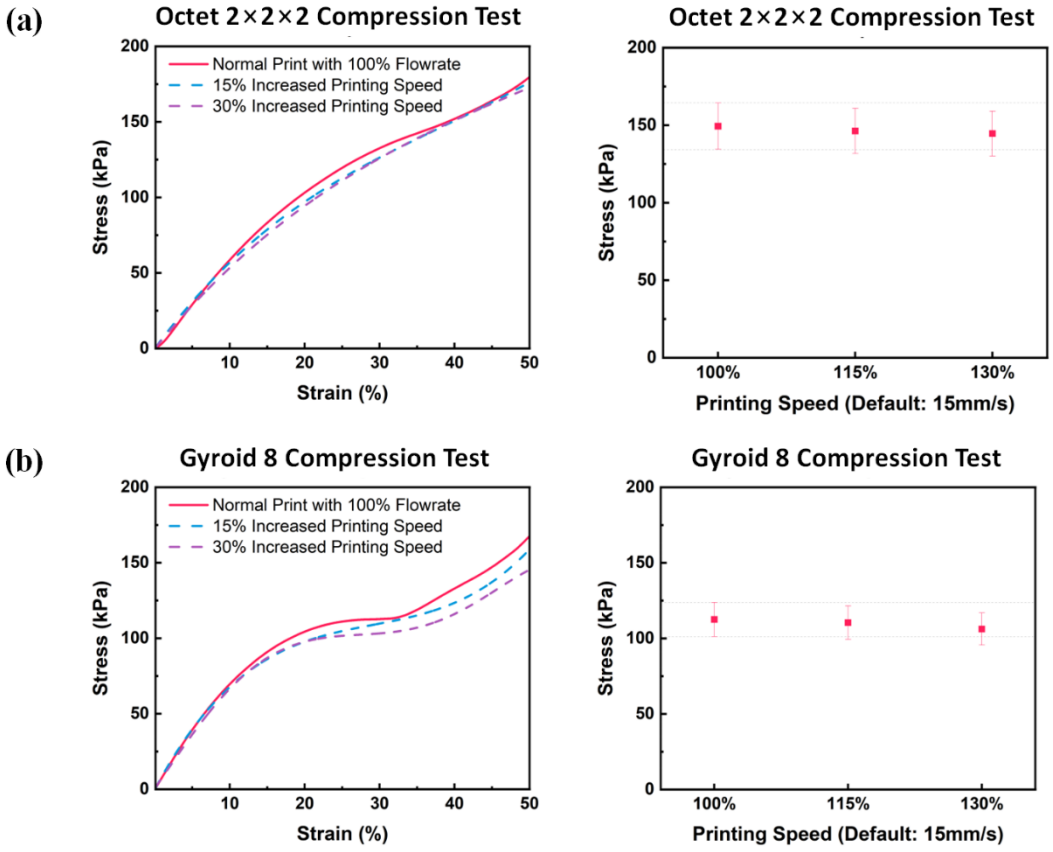

Figure 4.6. The rapid printing compression test results of (a) Octet 2×2×2 (b) Gyroid 8.

Figure 4.6 show the compression test results of the printed octets and gyroid with increased print speed, and the result shows that the yield strength found in all three cases lies within the error range. Table 4.1 shows the comparison of the printing time and compressive yield strength of the printed samples:

Table 4.1. Printing Time and Compressive Yield Strength of the Printed Models

Model	Printing Time		Compressive Yield Strength	
Octet 2×2×2	4hrs 24mins	–	112.55 kPa	–
	3hrs 44mins	– 15%	110.45 kPa	– 1.87%
	3hrs 5mins	– 30%	104.21 kPa	– 7.41%
Gyroid 8	3hrs 46mins	–	149.35 kPa	–
	3hrs 12mins	– 15%	146.31 kPa	– 2.04%
	2hrs 38mins	– 30%	144.60 kPa	– 3.18%

The results revealed that for the octet model, the printing time was reduced by 30 % from 4 hours to 1 hour and 19 minutes, but at the cost of a 7.41% decrease in compressive strength. Similarly, for the gyroid model, the printing time was saved by 30% from 4 hours to 1 hour and 8 minutes, however, the compressive strength was only reduced by 3.18%. This shows that the flexible material can still be fabricated faster but with little change of mechanical property within the error range.

Chapter 5. Conclusions and Future Work

5.1. Conclusions

The motivation, background, development process, and results of an intelligent rapid 3D printing system were demonstrated. The system was developed to address challenges associated with the flexible material, TPU, printing process using FDM, which was the main objective. Specifically, the defect occurrence and filament buckling phenomenon were investigated to enhance the fabrication process, particularly for TPU filaments. Test results showed that the developed system was able to adjust its flowrate and nozzle temperature based on in-situ data to reduce the occurrence of blobs or stringing defects. Furthermore, the system maintained sustained mechanical properties even at increased print speed without leading to printing failure for flexible material 3D printing process. The printing time was reduced by up to 30%, while maintaining mechanical properties within an error range of 3.18%.

In this research study, the primary objective was to design and develop the intelligent 3D printing assistant system with computer vision where it can control printing parameters to improve flexible material printing quality at an increased printing speed. Several achievements were accomplished in this thesis.

1. Selection of Primary and Supporting Printing Parameters

There are many different parameters that can be adjusted in-situ and ex-situ to improve quality of the 3D printed objects. The printing parameters that can be adjusted real-time during the fabrication process are printing speed, flowrate, nozzle temperature, print bed temperature, fan speed, and z-offset. Not only limited to the printing parameters, parameters such as layer height, wall thickness, infill settings, retraction, support structures, etc. can be adjusted prior to the printing process. In this study, the printing parameters that can be controlled along with the fabrication process were investigated and flowrate and nozzle temperature was found to have effect on the printing quality. Through the visual and compression tests, flowrate is selected to be the primary parameter and nozzle temperature to be supportive parameter. The flowrate shows the most effect on the printing process and the results where the nozzle temperature is required to be considered to ensure printability from the process.

2. Development of an Autonomous Parameter Control System

The autonomous parameter control system requires three main processes: 1) data acquisition 2) status identification 3) parameter control. The data acquisition process was completed by implementing the computer vision system to the commercial FDM printers. The acquired data is then passed to the status identification where CNN was utilized. The CNN was developed from scratch based on more than 50 combinations of hyperparameters such as kernel size and filter, number of convolutional layers, number of epochs, activations function, and optimizers and its learning rate. Based on the selected combinations showing the best results, the training accuracy showed 98.97% with the lowest classification accuracy for stringing defect. The output of the CNN model is provided as the percentage possibility of the pre-defined classes, in this case, stringing defect, blobs defect, normal print, and no information. The parameter control system was developed to control both flowrate and nozzle temperature based on the classification results to minimize defects while ensuring the printability.

3. Demonstration of the System

The performance of the developed system was validated through two types of testing methods, defect control test and rapid printing test. Throughout the study, two different types of structures are considered, 1D strut-based octet and 2D curve-based gyroid. The defect control test was performed by intentionally increasing or decreasing the flowrate every 25^{th} and 50^{th} layers to create blobs and stringing defects accordingly. During the demonstration, interesting phenomenon was observed which proves the correction accuracy between the models. Two different architectures showed continuous and discontinuous printing style where the octet showed discontinuous printing style and vice versa. The difference in printing style led to different changes in the printing process. Specifically in this research, the discontinuous printing of octet has higher occurrence rate of stringing defects as it is a common issue that arises during the nozzle travel between separated structures. The result demonstrated the importance of consideration in the printing style in the 3D printing process for the complex structures to minimize occurrence of defects.

The other test, rapid test was completed by incrementally increasing the print speed in between the batch of printing. From the first batch, the correction data was

recorded then mathematical correction was applied to the next batch of printing process. Throughout the test, the developed system led to sustain mechanical properties (compressive yield strength) at increased printing speed without leading to any printing failure. The printing time was reduced up to 30% while keeping the mechanical properties difference in the error range of 3.18%

5.2. Future Work

In this study, an autonomous 3D printing system for flexible materials was developed, which addresses the printability issue of flexible materials in 3D printing. The intelligent 3D printing system has the potential to be an affordable assistance system for optimizing the additive manufacturing process and can serve as the basis for future intelligent systems in the field. The system's ability to increase printing speed while minimizing defects and ensuring printability can be applied to various structures, making it a versatile solution.

The limitation of the developed system is the resolution of computer vision system which does not allow detection of microscopic defects on the print surface. By improving the computer vision system with higher resolution and optimized location, increasing the data size, and diversifying the CNN dataset to classify different types of defects, the defect control performance will be improved. Overall, this study provides a promising solution for advancing the additive manufacturing process with flexible materials.

References

[1] C. M. Thakar, S. S. Parkhe, A. Jain, K. Phasinam, G. Murugesan and R. J. M. Ventayen, "3d Printing: Basic principles and applications," *Materials Today: Proceedings,* vol. 51, no. 1, pp. 842-849, 2022.

[2] P. Holzmann, R. J. Breitenecker, A. A. Soomro and E. J. Schwarz, "User entrepreneur business models in 3D printing," *Journal of Manufacturing Technology Management,* vol. 28, no. 1, pp. 75-94, 2017.

[3] T.-H. Kim, X. Min, D. Baker, W. Lee and W. S. Kim, "3D architectured air sensing tubes for a portable mechanical ventilator," *Flexible and Printed Electronics,* vol. 6, no. 3, p. 035010, 2021.

[4] S. C. Joshi and A. A. Sheikh, "3D printing in aerospace and its long-term sustainability," *Virtual and physical prototyping,* vol. 10, no. 4, pp. 175-185, 2015.

[5] S. G. Sarvankar and S. N. Yewale, "Additive Manufacturing in Automobile Industry," *International Journal of Research in Aeronautical and Mechanical,* vol. 7, no. 4, pp. 01-10, 2019.

[6] J. N. Kok, E. J. Boers, W. A. Kosters, P. Van der Putten and M. Poel, "Artificial intelligence: definition, trends, techniques, and cases," *Artificial intelligence,* vol. 1, pp. 270-299, 2009.

[7] J. Li, R. Wang, J. Wang and Y. Li, "Analysis and forecasting of the oil consumption in China based on combination models optimized by artificial intelligence algorithms," *Energy,* vol. 144, pp. 243-264, 2018.

[8] Y. Dash, S. K. Mishra and B. K. Panigrahi, "Rainfall prediction for the Kerala state of India using artificial intelligence approaches," *Computers & Electrical Engineering,* vol. 70, pp. 66-73, 2018.

[9] B. Gong, J. P. Nugent, W. Guest, W. Parker, P. J. Chang, F. Khosa and S. Nicolaou, "Influence of artificial intelligence on Canadian medical students' preference for radiology specialty: ANational survey study," *Academic radiology,* vol. 4, no. 26, pp. 566-577, 2019.

[10] A. Tang, R. Tam, A. Cadrin-Chênevert, W. Guest, J. Chong, J. Barfett and Canadian Association of Radiologists (CAR) Artific, "Canadian Association of Radiologists white paper on artificial intelligence in radiology," *Canadian Association of Radiologists Journal,* vol. 2, no. 69, pp. 120-135, 2019.

[11] Y. Lu, "Artificial intelligence: a survey on evolution, models, applications and future trends," *Journal of Management Analytics ,* vol. 6, no. 1, pp. 1-29, 2019.

[12] A. Pandian and C. Belavek, "A review of recent trends and challenges in 3D printing," in *2016 ASEE North Central Section Conference*, Michigan, 2016.

[13] V. G. Gokhare, D. N. Raut and D. K. Shinde, "A review paper on 3D-printing aspects and various processes used in the 3D-printing," *International Journal of Engineering Research & Technology,* vol. 6, no. 6, pp. 953-958, 2017.

[14] K. V. Wong and A. Hernandez, "A review of additive manufacturing," *International scholarly research notices,* vol. 208760, p. 10, 2012.

[15] M. Tovey and J. Owen, "Sketching and direct CAD modelling in automotive design," *Design Studies,* vol. 6, no. 21, pp. 569-588, 2000.

[16] M. Tovey, "Drawing and CAD in industrial design," *Design Studies,* vol. 10, no. 1, pp. 24-39, 1989.

[17] R. A. Castellino, "Computer aided detection (CAD): an overview," *Cancer Imaging,* vol. 5, no. 1, p. 17, 2005.

[18] F. Remondino, "Heritage recording and 3D modeling with photogrammetry and 3D scanning," *Remote sensing,* vol. 3, no. 6, pp. 1104-1138, 2011.

[19] F. Remondino and S. El-Hakim, "Image-based 3D modelling: a review," *The photogrammetric record,* vol. 115, no. 21, pp. 269-291, 2006.

[20] Y. Song, Z. Yang, Y. Liu and J. Deng, "Function representation based slicer for 3D printing," *Computer Aided Geometric Design,* vol. 62, pp. 276-293, 2018.

[21] G. Z. Cheng, R. S. J. Estepar, E. Folch, J. Onieva, S. Gangadharan and A. Majid, "Three-dimensional printing and 3D slicer: powerful tools in understanding and treating structural lung disease," *Chest,* vol. 149, no. 5, pp. 1136-1142, 2016.

[22] J. C. Flowers, "Strong and Weak AI: Deweyan Considerations," *AAAI spring symposium: Towards conscious AI systems,* vol. 2287, no. 7, 2019.

[23] J. H. Moor, "The status and future of the Turing test," *Minds and Machines,* vol. 11, pp. 77-93, 2001.

[24] R. M. French, "The Turing Test: the first 50 years," *Trends in cognitive sciences,* vol. 4, no. 3, pp. 115-122, 2000.

[25] D. Keysers, T. Deselaers, C. Deselaers and H. Ney, "Deformation models for image recognition," *IEEE Transactions on Pattern Analysis and Machine Intelligence,* vol. 29, no. 8, pp. 1422-1435, 2007.

[26] G. K. Venayagamoorthy, V. Moonasar and K. Sandrasegaran, "Voice recognition using neural networks," in *Proceedings of the 1998 South*

African Symposium on Communications and Signal Processing-COMSIG'98, Rondebosch, 1998.

[27] A. Schlesinger, K. P. O'Hara and A. S. Taylor, "Let's talk about race: Identity, chatbots, and AI," in *Proceedings of the 2018 chi conference on human factors in computing systems*, QC, 2018.

[28] S. Robinson, J. S. Edwards and W. Yongfa, "Linking the Witness Simulation Software to an Expert System to Represent a Decision–Making Process," *Journal of Computing and Information Technology,* vol. 11, no. 2, pp. 123-133, 2003.

[29] M. A. S. Kamal, J. I. Imura, T. Hayakawa, A. Ohata and K. Aihara, "Smart driving of a vehicle using model predictive control for improving traffic flow," *IEEE Transactions on Intelligent Transportation Systems,* vol. 15, no. 2, pp. 878-888, 2014.

[30] J. Borana, "Applications of Artificial Intelligence & Associated Technologies," in *Science [ETEBMS-2016]*, 2016.

[31] I. S. 52900, Standard Terminology For Additive Manufacturing–General Principles–Part 1: Terminology, West Conshohocken: ASTM, 2015.

[32] M. Pagac, J. Hajnys, Q. P. Ma, L. Jancar, J. Jansa, P. Stefek and J. Mesicek, "A review of vat photopolymerization technology: materials, applications, challenges, and future trends of 3D printing," *Polymers,* vol. 13, no. 4, p. 598, 2021.

[33] F. Zhang, L. Zhu, Z. Li, S. Wang, J. Shi, W. Tang and J. Yang, "The recent development of vat photopolymerization: A review," *Additive Manufacturing,* vol. 48, p. 102423, 2021.

[34] M. Sireesha, J. Lee, A. S. K. Kiran, V. J. Babu, B. B. Kee and S. Ramakrishna, "A review on additive manufacturing and its way into the oil and gas industry," *RSC advances,* vol. 8, no. 40, pp. 22460-22468, 2018.

[35] Y. L. Yap, C. Wang, S. L. Sing, V. Dikshit, W. Y. Yeong and J. Wei, "Material jetting additive manufacturing: An experimental study using designed metrological benchmarks," *Precision engineering,* vol. 50, pp. 275-285, 2017.

[36] O. Gülcan, K. Günaydın and A. Tamer, "The state of the art of material jetting—a critical review," *Polymers,* vol. 13, no. 16, p. 2829, 2021.

[37] M. Ziaee and N. B. Crane, "Binder jetting: A review of process, materials, and methods," *Additive Manufacturing,* vol. 28, pp. 781-801, 2019.

[38] I. Gibson, B. Stucker, M. Khorasani, I. Gibson and D. Rosen, "Binder jetting," *Additive manufacturing technologies,* pp. 237-252, 2021.

[39] S. Sun, M. Brandt and M. J. L. A. M. Easton, "Powder bed fusion processes: An overview," *Laser additive manufacturing,* pp. 55-77, 2017.

[40] A. T. Sutton, C. S. Kriewall, M. C. Leu and J. W. Newkirk, "Powder characterisation techniques and effects of powder characteristics on part properties in powder-bed fusion processes," *Virtual and physical prototyping,* vol. 12, no. 1, pp. 3-29, 2017.

[41] I. Gibson, D. W. Rosen and B. Stucker, "Sheet lamination processes," *Additive manufacturing technologies: rapid prototyping to direct digital manufacturing,* pp. 223-252, 2010.

[42] P. M. Bhatt, A. M. Kabir, M. Peralta, H. A. Bruck and S. K. Gupta, "A robotic cell for performing sheet lamination-based additive manufacturing," *Additive Manufacturing,* vol. 27, pp. 278-289, 2019.

[43] D. G. Ahn, "Directed energy deposition (DED) process: state of the art," *International Journal of Precision Engineering and Manufacturing-Green Technology,* vol. 8, pp. 703-742, 2021.

[44] I. Gibson, D. Rosen and B. Stucker, "Directed energy deposition processes," *Additive manufacturing technologies: 3D printing, rapid prototyping, and direct digital manufacturing,* pp. 245-268.

[45] G. Hsiang Loh, E. Pei, J. Gonzalez-Gutierrez and M. Monzón, "An overview of material extrusion troubleshooting," *Applied Sciences,* vol. 10, no. 14, p. 4776, 2020.

[46] G. D. Goh, Y. L. Yap, H. K. J. Tan, S. L. Sing, G. L. Goh and W. Y. Yeong, "Process–structure–properties in polymer additive manufacturing via material extrusion: A review," *Critical Reviews in Solid State and Materials Sciences,* vol. 45, no. 2, pp. 113-133, 2020.

[47] S. Wickramasinghe, T. Do and P. Tran, "FDM-based 3D printing of polymer and associated composite: A review on mechanical properties, defects and treatments," *Polymers,* vol. 12, no. 7, p. 1529, 2020.

[48] T. Swetham, K. M. M. Reddy, A. Huggi and M. N. Kumar, "A Critical Review on of 3D Printing Materials and Details of Materials used in FDM," *Int. J. Sci. Res. Sci. Eng,* vol. 3, no. 2, pp. 353-361, 2017.

[49] H. Gong, D. Snelling, K. Kardel and A. Carrano, "Comparison of stainless steel 316L parts made by FDM-and SLM-based additive manufacturing processes," *Jom,* vol. 71, pp. 880-885, 2019.

[50] K. Günaydın and H. S. Türkmen, "Common FDM 3D printing defects," in *International Congress on 3D Printing (Additive Manufacturing) Technologies and Digital Industry*, 2018.

[51] Y. Tlegenov, W. F. Lu and G. S. Hong, "A dynamic model for current-based nozzle condition monitoring in fused deposition modelling," *Progress in Additive Manufacturing,* vol. 4, pp. 211-223, 2019.

[52] M. Wang, H. Zhang, Q. Hu, D. Liu and H. Lammer, "Research and implementation of a non-supporting 3D printing method based on 5-axis dynamic slice algorithm," *Robotics and Computer-Integrated Manufacturing,* vol. 57, pp. 496-505, 2019.

[53] H. Liu, L. Liu, D. Li, R. Huang and N. Dai, "An approach to partition workpiece CAD model towards 5-axis support-free 3D printing," *The International Journal of Advanced Manufacturing Technology,* vol. 106, pp. 683-699, 2020.

[54] M. Asif, J. H. Lee, M. J. Lin-Yip, S. Chiang, A. Levaslot, T. Giffney and K. C. Aw, "A new photopolymer extrusion 5-axis 3D printer," *Additive Manufacturing,* vol. 23, pp. 355-361, 2018.

[55] Ø. K. Grutle, *5-axis 3D Printer (Master's thesis),* University of Oslo, 2015.

[56] C. Bao, H. Moeinnia, T. H. Kim, W. Lee and W. S. Kim, "3D Structural Electronics Via Multi-Directional Robot 3D Printing," *Advanced Materials Technologies,* p. 2201349, 2022.

[57] J. Werner, M. Aburaia, A. Raschendorfer and M. Lackner, "MeshSlicer: A 3D-Printing software for printing 3D-models with a 6-axis industrial robot," *Procedia CIRP,* vol. 99, pp. 110-115, 2021.

[58] N. Oxman, J. Laucks, M. Kayser, E. Tsai and M. Firstenberg, "Freeform 3D printing: Towards a sustainable approach to additive manufacturing," *Green design, materials and manufacturing processes,* vol. 479, pp. 479-483, 2013.

[59] H. Al Jassmi, F. Al Najjar and A. H. I. Mourad, "Large-Scale 3D Printing: The Way Forward," in *IOP Conference Series: Materials Science and Engineering*, 2018.

[60] D. Bourell, J. P. Kruth, M. Leu, G. Levy, D. Rosen, A. M. Beese and A. Clare, "Materials for additive manufacturing," *CIRP annals,* vol. 66, no. 2, pp. 659-681, 2017.

[61] M. S. Xavier, A. J. Fleming and Y. K. Yong, "Finite element modeling of soft fluidic actuators: Overview and recent developments," *Advanced Intelligent Systems,* vol. 3, no. 2, p. 2000187, 2021.

[62] A. N. Gent, "On the relation between indentation hardness and Young's modulus," *Rubber Chemistry and Technology,* vol. 31, no. 4, pp. 896-906, 1958.

[63] I. M. Meththananda, S. Parker, M. P. Patel and M. Braden, "The relationship between Shore hardness of elastomeric dental materials and Young's modulus," *Dental materials,* vol. 25, no. 8, pp. 956-959, 2009.

[64] A. A. Ansari and M. Kamil, "Izod impact and hardness properties of 3D printed lightweight CF-reinforced PLA composites using design of experiment," *International Journal of Lightweight Materials and Manufacture,* vol. 5, no. 3, pp. 369-383, 2022.

[65] J. D. Kechagias, K. Ninikas, M. Petousis, N. Vidakis and N. Vaxevanidis, "An investigation of surface quality characteristics of 3D printed PLA plates cut by CO2 laser using experimental design," *Materials and Manufacturing Processes,* vol. 36, no. 13, pp. 1544-1553, 2021.

[66] L. Quiles-Carrillo, N. Montanes, F. Pineiro, A. Jorda-Vilaplana and S. Torres-Giner, "Ductility and toughness improvement of injection-molded compostable pieces of polylactide by melt blending with poly (ε-caprolactone) and thermoplastic starch," *Materials,* vol. 11, no. 11, p. 2138, 2018.

[67] J. Brandrup, E. H. Immergut, E. A. Grulke, A. Abe and D. R. Bloch, Polymer handbook, New York: Wiley, 1999.

[68] S. Hazer, M. Coban and A. Aytac, "A study on carbon fiber reinforced poly (lactic acid)/polycarbonate composites," *Journal of Applied Polymer Science,* vol. 135, no. 48, p. 46881, 2018.

[69] M. Spinu, C. Jackson, M. Y. Keating and K. H. Gardner, "Material design in poly (lactic acid) systems: block copolymers, star homo-and copolymers, and stereocomplexes," *Journal of Macromolecular Science, Part A: Pure and Applied Chemistry,* vol. 33, no. 10, pp. 1497-1530, 1996.

[70] M. Q. Tanveer, A. Haleem and M. Suhaib, "Effect of variable infill density on mechanical behaviour of 3-D printed PLA specimen: an experimental investigation," *SN Applied Sciences,* vol. 1, pp. 1-12, 2019.

[71] "Polylactic acid (PLA) properties," MatWeb , 2022. [Online]. Available: https://www.matweb.com/search/DataSheet.aspx?MatGUID=ab96a4c06 55c4018a8785ac4031b9278 &ckck=1. [Accessed 5th April 2022].

[72] X. Lin, J. Gao, J. Wang, R. Wang, M. Gong, L. Zhang and L. Zhang, "Desktop printing of 3D thermoplastic polyurethane parts with enhanced mechanical performance using filaments with varying stiffness," *Additive Manufacturing,* vol. 47, p. 102267, 2021.

[73] V. C. Chandrasekaran, "7 - Typical Rubber Testing Methods," in *Essential Rubber Formulary*, William Andrew Publishing, 2007, pp. 16-22.

[74] P. Poomalai and T. O. Varghese, "Thermomechanical Behaviour of Poly (methyl methacrylate)/Copoly (ether-ester) Blends," *International Scholarly Research Notices,* vol. 2011, p. 5, 2011.

[75] O. Poomalai and T. O. Varghese, "Investigation on thermoplastic co-poly (ether-ester) elastomer toughened poly (methylmethacrylate) blends," *Journal of applied polymer science,* vol. 109, no. 6, pp. 3511-3518, 2008.

[76] M. S. Zheng, J. W. Zha, Y. Yang, P. Han, C. H. Hu, Y. Q. Wen and Z. M. Dang, "Polyurethane induced high breakdown strength and high energy storage density in polyurethane/poly (vinylidene fluoride) composite films," *Applied Physics Letters,* vol. 110, no. 25, p. 252902, 2017.

[77] V. Jašo, M. Cvetinov, S. Rakić and Z. S. Petrović, "Bio-plastics and elastomers from polylactic acid/thermoplastic polyurethane blends," *Journal of Applied Polymer Science,* vol. 131, no. 22, 2014.

[78] M. Nofar, M. Mohammadi and P. J. Carreau, "Effect of TPU hard segment content on the rheological and mechanical properties of PLA/TPU blends," *Journal of Applied Polymer Science,* vol. 137, no. 45, p. 49387, 2020.

[79] Z. Liu, Y. Luo, H. Bai, Q. Zhang and Q. Fu, "Remarkably enhanced impact toughness and heat resistance of poly (L-lactide)/thermoplastic polyurethane blends by constructing stereocomplex crystallites in the matrix," *ACS Sustainable Chemistry & Engineering,* vol. 4, no. 1, pp. 111-120, 2016.

[80] "NinjaFlex 3D Printing Filament Technical Specifications," Ninjatek, April 2016. [Online]. Available: https://ninjatek.com/wp-content/uploads/NinjaFlex-TDS.pdf. [Accessed April 2022].

[81] M. Musioł, W. Sikorska, G. Adamus, H. Janeczek, J. Richert, R. Malinowski and M. Kowalczuk, "Forensic engineering of advanced polymeric materials. Part III-Biodegradation of thermoformed rigid PLA packaging under industrial composting conditions," *Waste Management,* vol. 52, pp. 69-76, 2016.

[82] M. Korger, A. Glogowsky, S. Sanduloff, C. Steinem, S. Huysman, B. Horn and M. Rabe, "Testing thermoplastic elastomers selected as flexible three-dimensional printing materials for functional garment and technical textile applications," *Journal of Engineered Fibers and Fabrics,* vol. 15, p. 1558925020924599, 2020.

[83] M. Galati and P. Minetola, "On the measure of the aesthetic quality of 3D printed plastic parts," *International Journal on Interactive Design and Manufacturing (IJIDeM),* vol. 14, pp. 381-392, 2020.

[84] L. R. Sbriglia, A. M. Baker, J. M. Thompson, R. V. Morgan, A. J. Wachtor and J. D. Bernardin, "Embedding sensors in FDM plastic parts during

additive manufacturing," in *Proceedings of the 34th IMAC, A Conference and Exposition on Structural Dynamics*, 2016.

[85] F. Osti, G. M. Osti, M. Neri, A. Liverani, L. Frizziero, S. Stilli and G. Trisolino, "CT conversion workflow for intraoperative usage of bony models: From DICOM data to 3D printed models," *Applied Sciences,* vol. 9, no. 4, p. 708, 2019.

[86] G. Cicala, D. Giordano, C. Tosto, G. Filippone, A. Recca and I. Blanco, "Polylactide (PLA) filaments a biobased solution for additive manufacturing: Correlating rheology and thermomechanical properties with printing quality," *Materials,* vol. 11, no. 7, p. 1191, 2018.

[87] K. Paraskevoudis, P. Karayannis and E. P. Koumoulos, "Real-time 3D printing remote defect detection (stringing) with computer vision and artificial intelligence," *Processes,* vol. 8, no. 11, p. 1464, 2020.

[88] K. Günaydın and H. S. Türkmen, "Common FDM 3D printing defects," in *International Congress on 3D Printing (Additive Manufacturing) Technologies and Digital Industry*, 2018.

[89] S. Naghieh and X. Chen, "Printability–A key issue in extrusion-based bioprinting," *Journal of Pharmaceutical Analysis,* vol. 11, no. 5, pp. 564-579, 2021.

[90] J. Forman, M. D. Dogan, H. Forsythe and H. Ishii, "DefeXtiles: 3D printing Quasi-Woven fabric via under-extrusion," in *Proceedings of the 33rd Annual ACM Symposium on User Interface Software and Technology*, 2020.

[91] M. Galati, P. Minetola, G. Marchiandi, E. Atzeni, F. Calignano, A. Salmi and L. Iuliano, "A methodology for evaluating the aesthetic quality of 3D printed parts," *Procedia CIRP,* vol. 79, pp. 95-100, 2019.

[92] A. Aitchison and Q. Wang, "Localised pre-heating to improve inter-layer delamination strength in fused deposition modelling," in *International Design Engineering Technical Conferences and Computers and Information in Engineering Conference*, 2019.

[93] G. Hsiang Loh, E. Pei, J. Gonzalez-Gutierrez and M. Monzón, "An overview of material extrusion troubleshooting," *Applied Sciences,* vol. 10, no. 14, p. 4776, 2020.

[94] J. Wächter, C. L. Elsner and E. Moritzer, "Investigation of Specific FDM Process Parameters to Optimize the Polymer Discharge of Carbon Fiber Reinforced PEEK," *Macromolecular Symposia,* vol. 395, no. 1, p. 2000269, 2021.

[95] Y. Tlegenov, Y. S. Wong and G. S. Hong, "A dynamic model for nozzle clog monitoring in fused deposition modelling," *Rapid Prototyping Journal,* vol. 23, no. 2, pp. 391-400, 2017.

[96] K. Singh Boparai, R. Singh and H. Singh, "Experimental investigations for development of Nylon6-Al-Al2O3 alternative FDM filament," *Rapid Prototyping Journal,* vol. 22, no. 2, pp. 217-224, 2016.

[97] A. Bellini, *Fused deposition modeling: a comprehensive experimental, analytical and computational study of material behavior, fabrication processand equipment design, PhD Thesis,* Drexel University, 2002.

[98] T. P. Paul and J. S. Batchelder, "Capacitive detector for use in extrusion-based digital manufacturing systems". Washington, DC Patent 8,222,908, 2012.

[99] Y. Arbaoui, P. Agaciak, A. Chevalier, V. Laur, A. Maalouf, J. Ville and P. Queffelec, "3D printed ferromagnetic composites for microwave applications," *Journal of Materials Science,* vol. 52, pp. 4988-4996, 2017.

[100] N. Kumar, P. K. Jain, P. Tandon and P. Mohan Pandey, "3D PRINTING OF FLEXIBLE PARTS USING EVA MATERIAL," *Materials Physics & Mechanics,* vol. 37, no. 2, 2018.

[101] C. Kousiatza and D. Karalekas, "In-situ monitoring of strain and temperature distributions during fused deposition modeling process," *Materials & Design,* vol. 97, pp. 400-406, 2016.

[102] Y. Tlegenov, G. S. Hong and W. F. Lu, "Nozzle condition monitoring in 3D printing," *Robotics and Computer-Integrated Manufacturing,* vol. 54, pp. 45-55, 2018.

[103] A. Dey and N. Yodo, "A systematic survey of FDM process parameter optimization and their influence on part characteristics," *Journal of Manufacturing and Materials Processing,* vol. 3, no. 3, p. 64, 2019.

[104] S. Kim, H. Seong, Y. Her and J. Chun, "A study of the development and improvement of fashion products using a FDM type 3D printer," *Fashion and Textiles,* vol. 6, no. 1, pp. 1-24, 2019.

[105] J. Žarko, G. Vladić, M. Pál and S. Dedijer, "Influence of printing speed on production of embossing tools using FDM 3D printing technology," *Journal of graphic engineering and design,* vol. 8, no. 1, pp. 19-27, 2017.

[106] X. Kuang, Z. Zhao, K. Chen, D. Fang, G. Kang and H. J. Qi, "High-speed 3D printing of high-performance thermosetting polymers via two-stage curing," *Macromolecular rapid communications,* vol. 39, no. 7, p. 1700809, 2018.

[107] A. Ceruti, A. Liverani and T. Bombardi, "Augmented vision and interactive monitoring in 3D printing process," *International Journal on Interactive Design and Manufacturing (IJIDeM),* vol. 11, pp. 385-395, 2017.

[108] E. R. Eiriksson, D. B. Pedersen, J. R. Frisvad, L. Skovmand, V. Heun, P. Maes and H. Aanæs, "Augmented reality interfaces for additive manufacturing," in *Image Analysis: 20th Scandinavian Conference, SCIA*, 2017.

[109] K. He, Q. Zhang and Y. Hong, "Profile monitoring based quality control method for fused deposition modeling process," *Journal of Intelligent Manufacturing,* vol. 30, pp. 947-958, 2019.

[110] M. Wu, V. V. Phoha, Y. B. Moon and A. K. Belman, "Detecting malicious defects in 3D printing process using machine learning and image classification," in *ASME International Mechanical Engineering Congress and Exposition*, 2016.

[111] H. Shen, W. Sun and J. Fu, "Multi-view online vision detection based on robot fused deposit modeling 3D printing technology," *Rapid Prototyping Journal,* vol. 25, no. 2, pp. 343-355, 2019.

[112] Y. Xin, L. Kong, Z. Liu, Y. Chen, Y. Li, H. Zhu and C. Wang, "Machine learning and deep learning methods for cybersecurity," *Ieee access,* vol. 6, pp. 35365-35381, 2018.

[113] I. El Naqa and M. J. Murphy, What is machine learning?, Springer International Publishing, 2015.

[114] P. P. Shinde and S. Shah, "A review of machine learning and deep learning applications," in *2018 Fourth international conference on computing communication control and automation (ICCUBEA)*, 2018.

[115] I. Goodfellow, Y. Bengio and A. Courville, Deep learning, MIT Press, 2016.

[116] C. Janiesch, P. Zschech and K. Heinrich, "Machine learning and deep learning," *Electronic Markets,* vol. 31, no. 3, pp. 685-695, 2021.

[117] C. Cortes and V. Vapnik, "Support vector machine," *Machine learning,* vol. 20, no. 3, pp. 273-297, 1995.

[118] Y. Freund and R. E. Schapire, "A decision-theoretic generalization of on-line learning and an application to boosting," *Journal of computer and system sciences,* vol. 55, no. 1, pp. 119-139, 1997.

[119] L. Breiman, "Random forests," *Machine learning,* vol. 45, pp. 5-32, 200.

[120] X. Chen, J. Tian, J. Cheng and X. Yang, "Segmentation of fingerprint images using linear classifier," *EURASIP Journal on Advances in Signal Processing,* pp. 1-15, 2004.

[121] M. P. LaValley, "Logistic regression," *Circulation,* vol. 117, no. 18, pp. 2395-2399, 2008.

[122] G. I. Webb, E. Keogh and R. Miikkulainen, "Naïve Bayes," *Encyclopedia of machine learning,* vol. 15, pp. 713-714, 2010.

[123] N. Friedman, D. Geiger and M. Goldszmidt, "Bayesian network classifiers," *Machine learning,* vol. 29, pp. 131-163, 1997.

[124] M. Pal, "Random forest classifier for remote sensing classification," *International journal of remote sensing,* vol. 26, no. 1, pp. 217-222, 2005.

[125] L. Breiman, "Bagging predictors," *Machine learning,* vol. 24, pp. 123-140, 1996.

[126] P. Cunningham and S. J. Delany, "k-Nearest neighbour classifiers-A Tutorial," *ACM computing surveys (CSUR),* vol. 54, no. 6, pp. 1-25, 2021.

[127] A. K. Jain, J. Mao and K. M. Mohiuddin, "Artificial neural networks: A tutorial," *Computer,* vol. 29, no. 3, pp. 31-44, 1996.

[128] R. A. Jarvis, "A perspective on range finding techniques for computer vision," *IEEE Transactions on Pattern Analysis and Machine Intelligence,* vol. 2, pp. 122-139, 1983.

[129] G. Stockman and L. G. Shapiro, Computer vision, Prentice Hall PTR, 2001.

[130] Y. LeCun, Y. Bengio and G. Hinton, "Deep learning," *Nature,* vol. 521, no. 7553, pp. 436-444, 215.

[131] L. Zhang, S. Wang and B. Liu, "Deep learning for sentiment analysis: A survey," *Wiley Interdisciplinary Reviews: Data Mining and Knowledge Discovery,* vol. 8, no. 4, p. e1253, 2018.

[132] N. Zhang, S. Ding, J. Zhang and Y. Xue, "An overview on restricted Boltzmann machines," *Neurocomputing,* vol. 275, pp. 1186-1199, 2018.

[133] L. R. Medsker and L. C. Jain, "Recurrent neural networks," *Design and Applications,* vol. 5, pp. 64-67, 2001.

[134] M. Schuster and K. K. Paliwal, "Bidirectional recurrent neural networks," *IEEE transactions on Signal Processing,* vol. 45, no. 11, pp. 2673-2681, 1997.

[135] S. Hochreiter and J. Schmidhuber, "Long short-term memory," *Neural computation,* vol. 9, no. 8, pp. 1735-1780, 1997.

[136] S. Lawrence, C. L. Giles, A. C. Tsoi and A. D. Back, "Face recognition: A convolutional neural-network approach," *IEEE transactions on neural networks,* vol. 8, no. 1, pp. 98-113, 1997.

[137] A. Jayanth Balaji, D. S. Harish Ram and B. B. Nair, "Applicability of Deep Learning Models for Stock Price Forecasting An Empirical Study on BANKEX Data," *Procedia Computer Science,* vol. 143, pp. 947-953, 2018.

[138] S. Ramaswamy and N. DeClerck, "Customer Perception Analysis Using Deep Learning and NLP," *Procedia Computer Science,* vol. 140, pp. 170-178, 2018.

[139] N. Kühl, M. Mühlthaler and M. Goutier , "Supporting customer-oriented marketing with artificial intelligence: automatically quantifying customer needs from social media," *Electronic Markets,* vol. 30, pp. 351-367, 2020.

[140] P. Abbeel, A. Coates, M. Quigley and A. Ng, "An application of reinforcement learning to aerobatic helicopter flight," *Advances in neural information processing systems,* p. 19, 2006.

[141] M. Abdullah, W. Iqbal and A. Erradi, "Unsupervised learning approach for web application auto-decomposition into microservices," *Journal of Systems and Software,* vol. 151, pp. 243-257, 2019.

[142] D. H. Wolpert, "The supervised learning no-free-lunch theorems," *Soft computing and industry: Recent applications,* pp. 25-42, 2002.

[143] Z. Ghahramani, "Unsupervised learning," in *Advanced Lectures on Machine Learning: ML Summer Schools 2003*, Tübingen, Canberra, 2004, pp. 72-112.

[144] L. P. Kaelbling, M. L. Littman and A. W. Moore, "Reinforcement learning: A survey," in *Journal of artificial intelligence research*, 4, 1996, pp. 237-285.

[145] J. Guo, J. Wu, Z. Sun, J. Long and S. Zhang, "Fault Diagnosis of Delta 3D Printers Using Transfer Support Vector Machine With Attitude Signals," *IEEE Access,* p. 2905264, 2019.

[146] S. J. Pan, I. W. Tsang, J. T. Kwok and Q. Yang, "Domain adaptation via transfer component analysis," *IEEE Trans. Neural Netw.,* vol. 22, no. 2, pp. 199-210, 2011.

[147] L. Li, R. McGuan, R. Isaac, P. Kavehpour and R. Candler, "Improving precision of material extrusion 3D printing by in-situ monitoring & predicting 3D geometric deviation using conditional adversarial networks," *Additive Manufacturing,* vol. 38, p. 101695, 2021.

[148] A. Bacha, A. H. Sabry and J. Benhra, "Fault Diagnosis in the Field of Additive Manufacturing (3D Printing) Using Bayesian Networks," *International Journal of Online & Biomedical Engineering,* vol. 15, no. 3, 2019.

[149] L. Scime and J. Beuth, "Anomaly detection and classification in a laser powder bed additive manufacturing process using a trained computer vision algorithm," *Additive Manufacturing,* vol. 19, pp. 114-126, 2018.

[150] Y. Zhang, G. S. Hong, D. Ye, K. Zhu and J. Y. Fuh, "Extraction and evaluation of melt pool, plume and spatter information for powder-bed fusion AM process monitoring," *Materials & Design,* vol. 156, pp. 458-469, 2018.

[151] W. Lee, J. Fritsch, A. Maqsood, S. Liu, T. Bourassa, R. Calara and W. S. Kim, "Adaptive 3D Printing for In Situ Adjustment of Mechanical Properties," *Advanced Intelligent Systems,* p. 2200229, 2022.

[152] Z. Jin, Z. Zhang and G. X. Gu, "Autonomous in-situ correction of fused deposition modeling printers using computer vision and deep learning," *Manufacturing Letters,* vol. 22, pp. 11-15, 2019.

[153] M. F. Khan, A. Alam, M. A. Siddiqui, M. S. Alam, Y. Rafat, N. Salik and I. Al-Saidan, "Real-time defect detection in 3D printing using machine learning," *Materials Today: Proceedings,* vol. 42, no. 2, pp. 521-528, 2021.

[154] L. Scime and J. Beuth, "A multi-scale convolutional neural network for autonomous anomaly detection and classification in a laser powder bed fusion additive manufacturing process," *Additive Manufacturing,* vol. 24, pp. 273-286, 2018.

[155] B. Yuan, G. M. Guss, A. C. Wilson, S. P. Hau-Riege, P. J. DePond, S. McMains and B. Giera, "Machine-learning-based monitoring of laser powder bed fusion," *Advanced Materials Technologies,* vol. 3, no. 12, p. 1800136, 2018.

[156] A. Khadilkar, J. Wang and R. Rai, "Deep learning–based stress prediction for bottom-up SLA 3D printing process," *The International Journal of Advanced Manufacturing Technology,* vol. 102, pp. 2555-2569, 2019.

[157] B. Maxfield, Maxfield, Essential Mathcad for engineering, science, and Math Ise, Burlington: Academic Press, 2009.

[158] Q. Xu, W. Li, Y. J. Yin, J. X. Zhou and H. Nan, "Finite element simulation of real cavity closure in cast Ti6Al4V alloy during hot isostatic pressing," *China Foundry,* vol. 19, no. 1, pp. 55-62, 2022.

[159] P. Athanker and A. Singh, "Finite Element Analysis and Failure Mechanisms of Porous Biomaterial Architecture for Prosthetic Device," in *Reliability and Risk Assessment in Engineering: Proceedings of INCRS 2018*, 2020.

[160] D. Li, W. Liao, N. Dai and Y. M. Xie, "Comparison of mechanical properties and energy absorption of sheet-based and strut-based gyroid cellular structures with graded densities," *Materials,* vol. 12, no. 13, p. 2183, 2019.

[161] Y. Jin, H. Kong, X. Zhou, G. Li and J. Du, "Design and characterization of sheet-based gyroid porous structures with bioinspired functional gradients," *Materials,* vol. 13, no. 17, p. 3844, 2020.

[162] K. Michielsen and D. G. Stavenga, "Gyroid cuticular structures in butterfly wing scales: biological photonic crystals," *Journal of The Royal Society Interface,* vol. 5, no. 18, pp. 85-94, 2008.

[163] P. Ferretti, C. Leon-Cardenas, G. M. Santi, M. Sali, E. Ciotti, L. Frizziero and A. Liverani, "Relationship between FDM 3D printing parameters study: parameter optimization for lower defects," *Polymers,* vol. 13, no. 13, p. 2190, 2021.

[164] G. Ćwikła, C. Grabowik, K. Kalinowski, I. Paprocka and P. Ociepka, "The influence of printing parameters on selected mechanical properties of FDM/FFF 3D-printed parts," in *IOP conference series: materials science and engineering*, 2017.

[165] S. Ding, B. Zou, P. Wang and H. Ding, "Effects of nozzle temperature and building orientation on mechanical properties and microstructure of PEEK and PEI printed by 3D-FDM," *Polymer Testing,* vol. 78, p. 105948, 2019.

[166] M. S. Alsoufi, M. W. Alhazmi, D. K. Suker, T. A. Alghamdi, R. A. Sabbagh, M. A. Felemban and F. K. Bazuhair, "Experimental characterization of the influence of nozzle temperature in FDM 3D printed pure PLA and advanced PLA+," *American Journal of Mechanical Engineering,* vol. 7, no. 2, pp. 45-60, 2019.

[167] b. Akhoundi, M. Nabipour, F. Hajami and D. Shakoori, "An experimental study of nozzle temperature and heat treatment (annealing) effects on mechanical properties of high-temperature polylactic acid in fused deposition modeling," *Polymer Engineering & Science,* vol. 60, no. 5, pp. 979-987, 2020.

[168] M. F. Ashby and R. M. Medalist, "The mechanical properties of cellular solids," *Metall Trans,* vol. A14, pp. 1755-1769, 1983.

[169] Y. Wang, J. Huang, Y. Wang, S. Feng, T. Peng, H. Yang and J. Zou, "A CNN-based adaptive surface monitoring system for fused deposition

modeling," *IEEE/ASME Transactions on Mechatronics,* vol. 25, no. 5, pp. 2287-2296, 2020.

[170] P. Cavalin and L. Oliveira, "Confusion matrix-based building of hierarchical classification," in *Progress in Pattern Recognition, Image Analysis, Computer Vision, and Applications: 23rd Iberoamerican Congress, CIARP 2018*, Madrid, Spain, 2019.

[171] T. Agrawal, R. Gupta and S. Narayanan, "On evaluating CNN representations for low resource medical image classification," in *ICASSP 2019-2019 IEEE International Conference on Acoustics, Speech and Signal Processing*, 2019.

[172] S. Bhagia, K. Bornani, R. Agrawal, A. Satlewal, J. Ďurkovič, R. Lagaňa and A. J. Ragauskas, "Critical review of FDM 3D printing of PLA biocomposites filled with biomass resources, characterization, biodegradability, upcycling and opportunities for biorefineries," *Applied Materials Today,* vol. 24, p. 101078, 2021.

[173] J. H. Park, H. K. Jung and J. R. Lee, "Development and evaluation of fall impact protection pads using additive manufacturing," *Materials,* vol. 12, no. 20, p. 3440, 2019.

Appendix A. CNN Training Process

Table A.1. CNN Training Results with Different Hyperparameter Combinations

Hyperparameter Combinations	Training Accuracy
K1A1O1-001 [EP-24]	86.50%
K1A1O2-001 [EP-22]	43.00%
K1A2O1-001 [EP-19]	42.00%
K1A2O2-001 [EP-25]	25.00%
K1A3O1-001 [EP-25]	25.00%
K1A3O2-001 [EP-25]	25.00%
K1A4O1-001 [EP-22]	64.75%
K1A4O2-001 [EP-17]	40.00%
K1A5O1-001 [EP-24]	75.00%
K1A5O2-001 [EP-23]	40.00%
K1A6O1-001 [EP-22]	66.50%
K1A6O2-001 [EP-23]	58.25%
K2A1O1-001 [EP-25]	85.00%
K2A1O2-001 [EP-17]	44.00%

Hyperparameter Combinations	Training Accuracy
K2A2O1-001 [EP-25]	25.00%
K2A2O2-001 [EP-25]	25.00%
K2A3O1-001 [EP-25]	25.00%
K2A3O2-001 [EP-25]	25.00%
K2A4O1-001 [EP-24]	76.00%
K2A4O2-001 [EP-22]	41.25%
K2A5O1-001 [EP-24]	72.00%
K2A5O2-001 [EP-24]	44.50%
K2A6O1-001 [EP-25]	86.00%
K2A6O2-001 [EP-20]	53.50%
K3A1O1-001 [EP-25]	64.75%
K3A1O2-001 [EP-22]	54.00%
K3A2O1-001 [EP-25]	25.00%
K3A2O2-001 [EP-25]	25.00%
K3A3O1-001 [EP-25]	25.00%
K3A3O2-001 [EP-25]	25.00%

Hyperparameter Combinations	Training Accuracy
K3A4O1-001 [EP-25]	25.00%
K3A4O2-001 [EP-25]	25.00%
K3A5O1-001 [EP-03]	38.25%
K3A5O2-001 [EP-25]	62.50%
K3A6O1-001 [EP-23]	82.00%
K3A6O2-001 [EP-25]	93.50%
K4A1O1-001 [EP-25]	93.00%
K4A1O2-001 [EP-23]	55.25%
K4A2O1-001 [EP-25]	25.00%
K4A2O2-001 [EP-25]	25.00%
K4A3O1-001 [EP-25]	25.00%
K4A3O2-001 [EP-25]	25.00%
K4A4O1-001 [EP-25]	25.00%
K4A4O2-001 [EP-25]	25.00%
K4A5O1-001 [EP-25]	25.00%
K4A5O2-001 [EP-25]	68.00%

Hyperparameter Combinations	Training Accuracy
K4A6O1-001 [EP-19]	73.25%
K4A6O2-001 [EP-22]	95.50%

Appendix B. CNN Development Code (Python)

```
import os, itertools, shutil, random, glob,
import numpy as np
import tensorflow as tf
from tensorflow.keras.models import Model
from tensorflow.keras.layers import Dense, Conv2D, Input, MaxPooling2D,
add, AveragePooling2D, GlobalMaxPooling2D
from tensorflow.keras.optimizers import Adam, SGD, RMSprop
from tensorflow.keras.preprocessing.image import ImageDataGenerator
from sklearn.metrics import confusion_matrix
import matplotlib.pyplot as plt
from pathlib import Path

#### GPU ONLY ####
physical_devices = tf.config.experimental.list_physical_devices('GPU')
tf.config.experimental.set_memory_growth(physical_devices[0], True)

#### Data Size Definition ####
train_datasize = 300
valid_datasize = 100
test_datasize = 20

#### Data Organization (Train, Valid, Test) ####
os.chdir('data/ExtrusionTest')
if os.path.isdir('train/normal') is False:
    os.makedirs('train/noinfo')
    os.makedirs('train/under')
    os.makedirs('train/normal')
    os.makedirs('train/over')
    os.makedirs('valid/noinfo')
    os.makedirs('valid/under')
    os.makedirs('valid/normal')
    os.makedirs('valid/over')
    os.makedirs('test/noinfo')
    os.makedirs('test/under')
    os.makedirs('test/normal')
    os.makedirs('test/over')
```

```
    for i in random.sample(glob.glob('normal*'), train_datasize):
        shutil.move(i, 'train/normal')
    for i in random.sample(glob.glob('noinfo*'), train_datasize):
        shutil.move(i, 'train/noinfo')
    for i in random.sample(glob.glob('over*'), train_datasize):
        shutil.move(i, 'train/over')
    for i in random.sample(glob.glob('under*'), train_datasize):
        shutil.move(i, 'train/under')
    for i in random.sample(glob.glob('normal*'), valid_datasize):
        shutil.move(i, 'valid/normal')
    for i in random.sample(glob.glob('noinfo*'), valid_datasize):
        shutil.move(i, 'valid/noinfo')
    for i in random.sample(glob.glob('over*'), valid_datasize):
        shutil.move(i, 'valid/over')
    for i in random.sample(glob.glob('under*'), valid_datasize):
        shutil.move(i, 'valid/under')
    for i in random.sample(glob.glob('normal*'), test_datasize):
        shutil.move(i, 'test/normal')
    for i in random.sample(glob.glob('noinfo*'), test_datasize):
        shutil.move(i, 'test/noinfo')
    for i in random.sample(glob.glob('over*'), test_datasize):
        shutil.move(i, 'test/over')
    for i in random.sample(glob.glob('under*'), test_datasize):
            shutil.move(i, 'test/under')

os.chdir('../../')

train_path = 'data/ExtrusionTest/train'
valid_path = 'data/ExtrusionTest/valid'
test_path = 'data/ExtrusionTest/test'
img_pix_size = 300

train_batches =
ImageDataGenerator(preprocessing_function=tf.keras.applications.mobilen
et.preprocess_input).flow_from_directory(directory=train_path,
target_size=(img_pix_size,img_pix_size), classes=['noinfo', 'normal',
'under', 'over'], batch_size=10)

valid_batches =
ImageDataGenerator(preprocessing_function=tf.keras.applications.mobilen
et.preprocess_input).flow_from_directory(directory=valid_path,
target_size=(img_pix_size,img_pix_size), classes=['noinfo', 'normal',
'under', 'over'], batch_size=10)

test_batches =
ImageDataGenerator(preprocessing_function=tf.keras.applications.mobilen
et.preprocess_input).flow_from_directory(directory=test_path,
target_size=(img_pix_size,img_pix_size), classes=['noinfo', 'normal',
'under', 'over'], batch_size=5, shuffle=False)


imgs, labels = next(train_batches)
```

```
#### Convolutional Neural Network Model Creation ####
CNN_Input = Input(shape=(img_pix_size,img_pix_size,1))
kernel_size = [16, 32, 64, 128, 256, 512,1024]
activations_func = 'selu'
total_types = 4 # Number of classes
epoch_num = 22 # Epoch number (Updated after the test)
opt_type = SGD
opt_learning_rate = 0.001

cnn_struct = Conv2D(kernel_size[0],5,activation=activations_func,
             padding = 'same')(CNN_Input)
cnn_struct = Conv2D(kernel_size[1], 3, activation=activations_func,
             padding = 'same')(cnn_struct)
cnn_struct = Conv2D(kernel_size[2], 3, activation=activations_func,
             padding = 'same')(cnn_struct)
cnn_struct = Conv2D(kernel_size[5], 5, activation=activations_func,
             padding = 'same')(cnn_struct)
block1_output = AveragePooling2D(pool_size=(2,2),strides=2)(cnn_struct)

cnn_struct = Conv2D(kernel_size[1], 5, activation=activations_func,
             padding = 'same')(block1_output)
cnn_struct = Conv2D(kernel_size[2], 3, activation=activations_func,
             padding = 'same')(cnn_struct)
cnn_struct = Conv2D(kernel_size[3], 3, activation=activations_func,
             padding = 'same')(cnn_struct)
cnn_struct = Conv2D(kernel_size[5], 3, activation=activations_func,
             padding = 'same')(cnn_struct)
block2_output = add([cnn_struct, block1_output])
block2_output = MaxPooling2D(pool_size=(2, 2),strides=2)(block2_output)

cnn_struct = Conv2D(kernel_size[2], 5, activation=activations_func,
             padding = 'same')(block2_output)
cnn_struct = Conv2D(kernel_size[3], 3, activation=activations_func,
             padding = 'same')(cnn_struct)
cnn_struct = Conv2D(kernel_size[4], 3, activation=activations_func,
             padding = 'same')(cnn_struct)
cnn_struct = Conv2D(kernel_size[5], 1, activation=activations_func,
             padding = 'same')(cnn_struct)
block3_output = add([cnn_struct, block2_output])
block3_output = MaxPooling2D(pool_size=(2, 2),strides=2)(block3_output)

cnn_struct = Conv2D(kernel_size[6], 1, activation=activations_func,
             padding = 'same')(block3_output)
cnn_struct = GlobalMaxPooling2D()(cnn_struct)
cnn_struct =
      Dense(kernel_size[6],activation=activations_func)(cnn_struct)
CNN_Output = Dense(total_types, activation='softmax')(cnn_struct)

model = Model(CNN_Input, CNN_Output)
```

```
model.summary()

model.compile(optimizer=opt_type(learning_rate=opt_learning_rate),
              loss='categorical_crossentropy', metrics=['accuracy'])

model.fit(x=train_batches,
    steps_per_epoch=len(train_batches),
    validation_data=valid_batches,
    validation_steps=len(valid_batches),
    epochs=epoch_num,
    verbose=2
)

test_imgs, test_labels = next(test_batches)

predictions = model.predict(x=test_batches, steps=len(test_batches),
              verbose=0)

print(np.round(predictions))

cm = confusion_matrix(y_true=test_batches.classes,
     y_pred=np.argmax(predictions, axis=-1))

cm_plot_labels = ['noinfo', 'normal', 'under', 'over']
plot_confusion_matrix(cm=cm, classes=cm_plot_labels, title='Confusion
Matrix')

#### Neural Network Model Exportation ####
# Model
model_structure = model.to_json()
file_path = Path("model_structure.json")
file_path.write_text(model_structure)
# Trained weight
model.save_weights("model_weight.h5")
```

Appendix C. Autonomous System PC Code

```
import os
import time
import socket
from ftplib import FTP

from PIL import Image, ImageDraw
from pathlib import Path
import numpy as np

from tensorflow.keras.models import model_from_json
from tensorflow.keras.preprocessing import image
from tensorflow.keras.applications.mobilenet import preprocess_input

TCP_IP = '192.168.137.1'
TCP_PORT = 5005
TCP_CONNECTION = (TCP_IP,TCP_PORT)

#### Image Retrieval from Pi ####
def Take_snapshot():
    server = socket.socket(socket.AF_INET, socket.SOCK_STREAM)
    server.bind(TCP_CONNECTION)
    server.listen(1)
    conn, addr = server.accept()
```

```
while True:
        data = conn.recv(1024)
        if data == b"1":
            #### FTP Connection ####
            ftp = FTP('192.168.137.19')
            ftp.login('pi','raspberry')
            ftp.cwd('~/scripts/cnn_application')
            with open('snapshot.jpg', 'wb') as fp:
                ftp.retrbinary('RETR snapshot.jpg', fp.write)
            ftp.quit()

            #### Image Process ####
            with Image.open('snapshot.jpg') as im:
               image_size = (20, 100, 320, 400)  # x1 y1 x2 y2

               top_cover = [(0, 0), (22, 640)]
               nozzle_cover = [(22, 215), (22, 285), (52, 250)]

               ImageDraw.Draw(im).rectangle(top_cover, fill="black",
                                                 outline="black")
               ImageDraw.Draw(im).polygon(nozzle_cover, fill="black",
                                  outline="black")


               im.crop(image_size).transpose(Image.Transpose.ROTATE_270
               ).save('snapshot.jpg', format='jpeg')

            break
    conn.close()
    server.close()
```

```
#### Image Classification ####
    image_path = "snapshot.jpg"

    file_path = Path("9700accuracy/model_structure.json")
    model_structure = file_path.read_text()
    model = model_from_json(model_structure)
    model.load_weights("9700accuracy/model_weight.h5")
    img = image.load_img(image_path, target_size=(300, 300))
    img_array = image.img_to_array(img)
    img_batch = np.expand_dims(img_array, axis=0)
    img_preprocessed = preprocess_input(img_batch)
    predictions = model.predict(img_preprocessed)
    class_number = np.argmax(predictions[0])
    likelihood = np.max(predictions[0])
    class_names = {
        0: "No Information Found",
        1: "Normal Extrusion",
        2: "Stringing Defect",
        3: "Blobs Defect"

#### Classification Data Transfer ####
def Result_Transfer(defect_class):

    if defect_class == 2:
        message = b"String"
    elif defect_class == 3:
        message = b"Blob"
    else:
        message = b"NA"

    server = socket.socket(socket.AF_INET, socket.SOCK_STREAM)
    server.bind(TCP_CONNECTION)
    server.listen(1)
```

```
    conn, addr = server.accept()

    conn.sendall(message)
    data = conn.recv(1024)

    if data:
        conn.close()
        server.close()

#### Main ####
if __name__=='__main__':
   while True:
      Take_snapshot()
      time.sleep(2)
      defect_class = Defect_Detection()
      Result_Transfer(defect_class)
      time.sleep(10)
```

Appendix D. Autonomous System Pi Code

```
import os
import socket
import serial
import time

TCP_IP = '192.168.137.1'
TCP_PORT = 5005
TCP_ADDR = (TCP_IP, TCP_PORT)
Data_Tracking = 0

Flowrate = 100
Temperature = 228

FILENAME = 'snapshot.jpg'
BUFFER_SIZE = 4096

#### Image Data Transfer to PC ####
def Image_Send_PC():
      client = socket.socket(socket.AF_INET, socket.SOCK_STREAM)
      client.connect(TCP_ADDR)

      client.sendall(b'1')
      time.sleep(2)
      client.close()

      os.system("sh remove_snapshot.sh")

#### Connection-over-internet Establishment ####
def Test_Connection():

      if os.path.exists('/dev/ttyUSB0') == True:
            signal = serial.Serial(
            port='/dev/ttyUSB0',
            baudrate=250000,
            timeout=10000)
      else:
            signal = 0

      return signal
```

```
#### Printer Control ####
def Printer_Control():
      global Data_Tracking, Flowrate, Temperature

      client = socket.socket(socket.AF_INET, socket.SOCK_STREAM)
      client.connect(TCP_ADDR)

      data = client.recv(1024)

      if data:
            client.sendall(b'1')
            client.close()

      signal = Test_Connection()

      print("Data Recevied")
      while signal == 0:
            signal = Test_Connection()

      if signal != 0:
            print("Signal Established")

      control_update = open('control_data.txt', 'a+')

      if Data_Tracking%FORCE_LAYER == 0:
            if Data_Tracking == 0 or Data_Tracking == 125:
                  control_update.write(f'{Data_Tracking}, Flowrate,
{Flowrate},
                                    Temperature, {Temperature}\n')
                  signal.write(bytes(f"M221 S{Flowrate}\r\n", 'utf-8'))
                  signal.write(bytes(f"M104 S{Temperature}\r\n", 'utf-
8'))
            else:
                  Flowrate = 85
                  Temperature = 228
                  signal.write(bytes(f"M221 S{Flowrate}\r\n", 'utf-8'))
                  signal.write(bytes(f"M104 S{Temperature}\r\n", 'utf-
8'))
                  control_update.write(f'{Data_Tracking}, Flowrate,
{Flowrate},
                                    Temperature, {Temperature}\n')
```

```
	else:
		if data == b"String":
			Flowrate += 1
			Temperature += 1
			if Flowrate > 115:
				Flowrate = 115
			if Temperature > 233:
				Temperature = 233

			signal.write(bytes(f"M221 S{Flowrate}\r\n", 'utf-8'))
			signal.write(bytes(f"M104 S{Temperature}\r\n", 'utf-
8'))

		elif data == b"Blob":
			print("Over extrusion detected")
			Flowrate -= 1
			Temperature -= 1
			if Flowrate < 85:
				Flowrate = 85
			if Temperature < 227:
				Temperature = 227

			signal.write(bytes(f"M221 S{Flowrate}\r\n", 'utf-8'))
			signal.write(bytes(f"M104 S{Temperature}\r\n", 'utf-
8'))

		else:
			control_update.write(f'{Data_Tracking}, Flowrate,
{Flowrate},
					Temperature, {Temperature}\n')

	Data_Tracking += 1
	control_update.close()


#### Main ####
if __name__=='__main__':
	while True:
		# os.system("sh take_snapshot.sh")
		if os.path.exists(FILENAME) == True:
			Image_Send_PC()
			Printer_Control()
		else:
			time.sleep(5)
```